Remote Sensing of Environment 280 (2022) 113180

Contents lists available at ScienceDirect

Remote Sensing of Environment

journal homepage: www.elsevier.com/locate/rse

Non-destructive estimation of individual tree biomass: Allometric models, terrestrial and UAV laser scanning

Benjamin Brede [a,b,*], Louise Terryn [c], Nicolas Barbier [d], Harm M. Bartholomeus [a], Renée Bartolo [e], Kim Calders [c], Géraldine Derroire [g], Sruthi M. Krishna Moorthy [c,f], Alvaro Lau [a], Shaun R. Levick [h], Pasi Raumonen [i], Hans Verbeeck [c], Di Wang [j], Tim Whiteside [e], Jens van der Zee [a], Martin Herold [a,b]

[a] Wageningen University & Research, Laboratory of Geo-Information Science and Remote Sensing, Droevendaalsesteeg 3, 6708 PB Wageningen, The Netherlands
[b] Helmholtz Center Potsdam GFZ German Research Centre for Geosciences, Section 1.4 Remote Sensing and Geoinformatics, Telegrafenberg, 14473 Potsdam, Germany
[c] CAVElab – Computational & Applied Vegetation Ecology, Department of Environment, Ghent University, Coupure Links 653, 9000 Gent, Belgium
[d] Botany and Modelling of Plant Architecture and Vegetation (AMAP) Laboratory, French National Research Institute for Sustainable Development (IRD), Center for International Cooperation in Agricultural Research for Development (CIRAD), Scientific Research National Center (CNRS), Institut national de la recherche agronomique (INRA), Montpellier University, Montpellier, France
[e] Department of Agriculture, Water and the Environment, Supervising Scientist Branch, Darwin 0820, NT, Australia
[f] Department of Geographical Sciences, University of Maryland, College Park, USA
[g] CIRAD, UMR EcoFoG (Agroparistech, CNRS, INRAE, Université des Antilles, Université de la Guyane), Kourou, French Guiana, France
[h] CSIRO Land and Water, PMB 44, Winnellie 0822, NT, Australia
[i] Mathematics, Tampere University, Korkeakoulunkatu 1, 33720 Tampere, Finland
[j] Department of Remote Sensing Science and Technology, School of Electronic Engineering, Xidian University, Xi'an 710077, China

ARTICLE INFO

Edited by Jing M. Chen

Keywords:
Terrestrial laser scanning (TLS)
Unoccupied aerial vehicle laser scanning (UAV-LS)
Quantitative structure modelling (QSM)
Forest
Aboveground biomass (AGB)
Allometric scaling model (ASM)

ABSTRACT

Calibration and validation of aboveground biomass (AGB) (AGB) products retrieved from satellite-borne sensors require accurate AGB estimates across hectare scales (1 to 100 ha). Recent studies recommend making use of non-destructive terrestrial laser scanning (TLS) based techniques for individual tree AGB estimation that provide unbiased AGB predictors. However, applying these techniques across large sites and landscapes remains logistically challenging. Unoccupied aerial vehicle laser scanning (UAV-LS) has the potential to address this through the collection of high density point clouds across many hectares, but estimation of individual tree AGB based on these data has been challenging so far, especially in dense tropical canopies. In this study, we investigated how TLS and UAV-LS can be used for this purpose by testing different modelling strategies with data availability and modelling framework requirements. The study included data from four forested sites across three biomes: temperate, wet tropical, and tropical savanna. At each site, coincident TLS and UAV-LS campaigns were conducted. Diameter at breast height (DBH) and tree height were estimated from TLS point clouds. Individual tree AGB was estimated for ≥170 trees per site based on TLS tree point clouds and quantitative structure modelling (QSM), and treated as the best available, non-destructive estimate of AGB in the absence of direct, destructive measurements. Individual trees were automatically segmented from the UAV-LS point clouds using a shortest-path algorithm on the full 3D point cloud. Predictions were evaluated in terms of individual tree root mean square error (RMSE) and population bias, the latter being the absolute difference between total tree sample population TLS QSM estimated AGB and predicted AGB. The application of global allometric scaling models (ASM) at local scale and across data modalities, i.e., field-inventory and light detection and ranging LiDAR metrics, resulted in individual tree prediction errors in the range of reported studies, but relatively high population bias. The use of adjustment factors should be considered to translate between data modalities. When calibrating local models, DBH was confirmed as a strong predictor of AGB, and useful when scaling AGB estimates with field inventories. The combination of UAV-LS derived tree metrics with non-parametric modelling generally produced high individual tree RMSE, but very low population bias of ≤5% across sites starting from 55 training samples. UAV-LS has the potential to scale AGB estimates across hectares with reduced fieldwork time.

* Corresponding author at: Helmholtz Center Potsdam GFZ German Research Centre for Geosciences, Section 1.4 Remote Sensing and Geoinformatics, Telegrafenberg, 14473 Potsdam, Germany.
E-mail address: benjamin.brede@gfz-potsdam.de (B. Brede).

https://doi.org/10.1016/j.rse.2022.113180
Received 29 October 2021; Received in revised form 4 July 2022; Accepted 16 July 2022
Available online 5 August 2022

Overall, this study contributes to the exploitation of TLS and UAV-LS for hectare scale, non-destructive AGB estimation relevant for the calibration and validation of space-borne missions targeting AGB estimation.

1. Introduction

Recent and upcoming satellite missions targeting the estimation of forest aboveground biomass (AGB) such as BIOMASS, GEDI, NISAR and ALOS-4 require accurate and extensive calibration and validation data (Duncanson et al., 2019). A range of methods have been proposed that aim at area-wide AGB estimation with varying accuracy and acquisition speeds. Traditional field methods applied in forest inventories are based on field-measurable tree metrics like diameter at breast height DBHand tree height, combined with allometric scaling models (ASM) calibrated on destructively harvested individuals and are grounded in allometric scaling theory (Picard et al., 2012). These tree metrics are already collected in plot networks that have a large geographical coverage (Chave et al., 2004, 2005; Réjou-Méchain et al., 2017). However, large trees pose a problem as they are rarely harvested and hence not well represented in ASM (Duncanson et al., 2019; Burt et al., 2020; Disney et al., 2018). Additionally, recent studies discuss if allometric scaling laws actually still hold for large trees (Burt et al., 2020, 2021).

Airborne laser scanning (ALS) collects of point clouds that characterise the forest canopy structure at the landscape-scale. From this structural information, AGB can be inferred over large areas through either area-based or tree-centric approaches, thereby making it attractive for satellite mission calibration and validation. For area-based approaches, canopy vertical structure metrics such as top of canopy height are derived and calibrated with local field derived AGB at the plot scale to predict AGB (Asner and Mascaro, 2014). Area-based approaches are typically calibrated for one specific product resolution only. Additionally, edge effects result in larger estimation errors at fine resolution and cancel out when aggregating to coarser resolution, effectively making the prediction errors scale-dependent (Mascaro et al., 2011; Knapp et al., 2021; Réjou-Méchain et al., 2019).

For tree-centric approaches, individual trees are identified in the ALS point cloud with segmentation routines. Individual tree metrics such as individual tree height and crown diameter can then be estimated for the segmented trees, and subsequently used in combination with ASM to derive AGB at the tree level. Finally, the individual tree AGB is summed across an area to derive the plot AGB. This approach is very similar to well-known traditional ASM approaches of field plots (Coomes et al., 2017) and is independent of the scale of calibration plots (Dalponte and Coomes, 2016). However, a challenge for tree-centric approaches with ALS data is the delineation of crowns as well as the identification of understorey trees (Coomes et al., 2017). Moreover, tree-centric approaches require much higher point density than area-based approaches. Both area-based and tree-centric approaches rely on ASM calibrated against destructively harvested trees. The sampling of the respective harvest trees is often biased towards small trees and errors are often not characterised (Disney et al., 2018).

Terrestrial laser scanning (TLS) was discussed as a preferred data source for forest AGB validation (Duncanson et al., 2019) and a potential new standard for assessment of forest structural metrics (Levick et al., 2021; Brede et al., 2017). In essence, high-density point clouds are collected with a TLS instrument from the ground. From these point clouds, single trees are segmented and subsequently explicit geometric models are built (Raumonen et al., 2015; Hackenberg et al., 2015). These models serve to estimate individual tree wood volume, which in combination with wood density can estimate AGB. Hence, TLS is not a direct measurement of tree AGB, and should not be treated as such. Some studies suggest that TLS could provide unbiased individual tree AGB estimation with errors independent of tree size and low bias (±10%) (Calders et al., 2015; Stovall et al., 2017; Demol et al., 2021b), while others showed increase of error with tree size (Gonzalez de Tanago et al., 2018; Momo Takoudjou et al., 2018). Demol et al. (2022) listed eleven studies that include in total 303 individual trees and employed TLS to estimate individual tree AGB. All eleven were able to produce a plot bias of ≤10% compared to destructive measurements and eight even a bias ≤5%. Current shortcomings of TLS-based AGB estimation include uncertainty on tree-internal variation of wood density (Demol et al., 2021a), volume estimation of small branches (<10 cm in diameter) (Demol et al., 2022; Wilkes et al., 2021), variability of wood density within individual trees (Demol et al., 2021a) and variability in estimation of automatic processing pipelines (Momo Takoudjou et al., 2018; Martin-Ducup et al., 2021). Nonetheless, to date TLS appears to be the best non-destructive estimate for individual tree AGB in the absence of direct, destructive measurements. Still, in terms of satellite calibration and validation, time spent in the field of 3–7 days ha^{-1} and a lack of reliable individual tree segmentation algorithms suitable for complex tropical canopies are major bottlenecks (Wilkes et al., 2017). These issues make large-scale calibration and validation based on TLS sample plots still unfeasible.

From the early 2010s, unoccupied aerial vehicle laser scanning (UAV-LS) systems[1] have been investigated for forest structural characterisation across hectare scales (1–100 ha). While initial systems were primarily custom-built (Jaakkola et al., 2010; Wallace et al., 2012; Guo et al., 2017), commercial systems became available from the mid 2010s (Mandlburger et al., 2015; Brede et al., 2017; Wieser et al., 2017). Basic forestry metrics like DBH, canopy height and tree count have already been successfully derived (Brede et al., 2017; Wallace et al., 2014; Wieser et al., 2017), and explicit geometric modelling with quantitative structure modellings (QSM) has been attempted (Brede et al., 2019). In the context of tree volume and AGB estimation, a major challenge is the detection of lower canopy elements with UAV-LS, specifically trunks that contain most of trees' AGB. In particular DBH, which is often used in field-based ASM, could be reliably estimated in Norway spruce and Scots pine stands (Kuželka et al., 2020), but not in heterogeneous stands due to the lack of sufficient trunk points resulting from the top-of-canopy perspective (Brede et al., 2017; Levick et al., 2021; Vandendaele et al., 2021; Terryn et al., 2022). Hence, other tree metrics need to be exploited to estimate tree volume. For example, Puliti et al. (2020) presented an approach that estimates growing stock volume based solely on UAV-LS. They identified trees that permitted DBH estimation, and trained local prediction models between UAV-LS estimated tree height and DBH. This made it possible to estimate DBH for all trees within the plot and hence application of field-derived ASM for total tree wood volume. However, this approach is limited to forests that enable DBH estimation of a sufficient number of trees, which is usually only the case for open, structurally less complex forests.

The overall objective of this study was to test modelling strategies based on TLS and UAV-LS technologies for non-destructive estimation of individual tree AGB. Specifically, calibration strategies involving globally and locally calibrated prediction models were distinguished. Global approaches are cost-efficient, because no calibration samples need to be collected locally, and were tested to assess their performance at the available sites. As the application of globally calibrated ASM at the local scale currently includes the crossing of measurement modalities, i.e., between field- and laser scanning measurements, the consequence on the prediction was investigated. On the other hand, local approaches were tested with the setup of supersites in mind, where high quality calibration samples can be invested in. In this scenario, the question was which measurements – field-inventory, TLS or UAV-LS – combined with

[1] For a discussion on UAV terminology see (Joyce et al., 2021).

modelling approaches can yield the best performance for a supersite tree population. Field measurements can be regarded as relatively cost-efficient and require less investments in technology and training than light detection and ranging (LiDAR) approaches. Additionally, vast amounts of inventory data are already available across research plots and in national forest inventories (NFI), which can be used for satellite calibration and validation. For UAV-LS the limitation to reliably detect the tree trunks had to be considered. Finally, in the case of locally calibrated scaling models, the number of necessary calibration samples was investigated as they determine the number of TLS samples required. The focus of this study was to explore different modelling strategies for individual tree AGB (in Mg), not plot scale AGB (in Mg ha^{-1}).

2. Data

2.1. Study sites and campaigns

Four study sites, for which high quality UAV-LS and TLS data were available, were included in this study. These sites were located in Europe, South America, and Australia, and represent a variety of forest types and tree architectures (Figs. 1 and 2).

2.1.1. Speulderbos, The Netherlands (NL)

The Speulderbos Reference site is located in the Veluwe forest area in the Netherlands (Brede et al., 2016, N52° 15.15′ E5° 42.00′). The core stand of the site consists mainly of mature European beech (*Fagus sylvatica*) and oak (*Quercus robur*, *Q. petraea*) with sparse understorey. Adjacent to this core stand are gymnosperm stands of Norway spruce (*Picea abies*), Giant fir (*Abies grandis*) and Douglas fir (*Pseudotsuga menziesii*) (Brede et al., 2017, 2019). In the context of this study, Speulderbos (NL) is an example for mature, temperate forests with small amounts of understorey. Data collection covered the core and adjacent gymnosperm stands, and was carried out on 10 May (UAV-LS), 8 and 10 May 2017 (TLS) (Brede et al., 2020).

2.1.2. Paracou, French Guiana (FG)

The Paracou Research Station is situated in a lowland tropical *terra firme* forest of the Guiana Shield and home to more than 750 woody species (N°5 18′ W52° 53′, https://paracou.cirad.fr/). The station was initiated in 1984 with a large-scale controlled disturbance experiment across 12 plots with each 6.25 ha between 1986 and 1988. The focus in this study was on plot 6, which was a control plot during the disturbance experiment, i.e., it was left intact and without treatment. Plot 6 had a stem density of 563 ha^{-1} (DBH ≥10 cm) and AGB density of 421.9 Mg ha^{-1} in 2017 according to census data. Lianas are present throughout the plot at low levels and the plot has a healthy understorey layer. During a combined TLS and UAV-LS campaign data were collected in plot 6 between 10 October and 15 November 2019. A quadratic area with 200 m side length covering the NE corner of plot 6 was scanned first with UAV-LS, then with TLS (Fig. 3). FG was selected as an example for a dense tropical rainforest.

2.1.3. Robson Creek, Australia (RC)

The RC 25 ha rainforest plot was established in 2009 as the centrepiece of the Robson Creek node of the Far North Queensland Rainforest Supersite (Bradford et al., 2014). The RC site is located in a simple to complex notophyll vine forest in NE Queensland, Australia (S17°7′ E145°37′). The site is an Oz-flux site and supersite within the Terrestrial Ecosystem Research Network (TERN) (https://www.tern.org.au/tern-observatory/tern-ecosystem-processes/robson-creek-rainforest-supersite/). The 25 ha plot was selectively logged with the last logging undertaken between 1960 and 1969 (Bradford et al., 2014). The focus in this study was on the single core hectare (hectare number 6) which is located on the western edge of the 25 ha plot. This hectare had a stem density of 967 ha (DBH ≥10 cm) according to census data from 2019. Lianas are present throughout the plot and the plot has a healthy understory layer.

TLS data were collected in July and August 2018, with UAV-LS collection following on 18 and 19 September 2018. Of the two flights used in this study, one covered only the TLS plot at 2.5 m s^{-1}, while the other also covered the surrounding area at 8 m s^{-1}. This and the fewer number of flights when compared to FG, led to about half the point density as at FG (Table 1). The point cloud densities of FG and RC were not harmonised in order to investigate the effect of point cloud density on prediction performance.

2.1.4. Litchfield, Australia (LF)

The LF site (S13°10.74′ E130°47.67′) has a wet–dry tropical climate with a pronounced rain season between November and April (Luck et al., 2020). LF is dominated by Darwin woollybutt (*Eucalyptus miniata*) and can be classified as tropical savanna. Like RC, LF is a supersite and part of OzFlux and TERN (https://www.tern.org.au/tern-observatory/tern-ecosystem-processes/litchfield-savanna-supersite/). The TLS campaign that included RC also covered LF in July and August 2018. UAV-LS was collected on 12 and 13 September 2018.

2.2. TLS protocol

TLS data collection was performed with different RIEGL VZ-400 scanners across the four sites (Table 2). The VZ-400 has been used in several studies targeting individual tree AGB estimation (Calders et al., 2015; Gonzalez de Tanago et al., 2018; Lau et al., 2019) and ranging

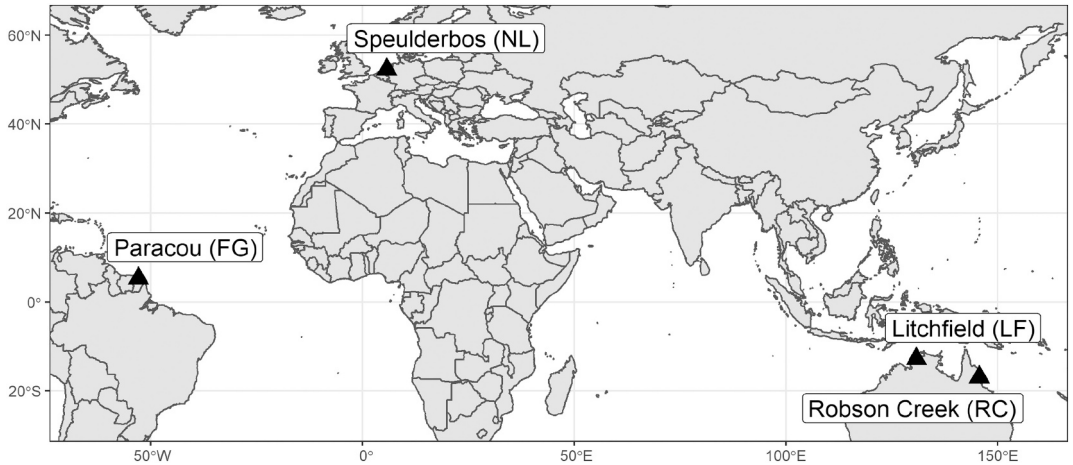

Fig. 1. Site locations.

(a) NL (b) FG

(c) RC (d) LF

Fig. 2. Impressions from the study sites. NL shows the young beech part of the plot. At LF, a RIEGL VZ-400 is installed on tripod during scanning.

accuracy has been found to be comparable among the different devices (Calders et al., 2017). TLS data collection and processing followed standard procedures for large area forest scanning (Wilkes et al., 2017). Regular grids of scan positions with variable grid spacing depending on forest density and complexity were implemented (Table 1). At each position, scans with the scanner in upright and horizontal tilting were performed by using the VZ-400 tilt-mount. Retro-reflective targets were placed in between consecutive scans in order to facilitate coarse registration. Co-registration between individual scan positions was performed with RIEGL's RiSCAN PRO software first with the help of the retro-reflectors for coarse registration, then using the Multi-Station Adjustment (MSA) routine for fine registration (Wilkes et al., 2017). This routine first searches for planar surfaces in the scan data, which can be tree trunk surfaces or ground patches. Then, these surfaces are used as registration targets to adjust the scan position of all individual scans of the scan project. Due to lack of reliable global navigation satellite system (GNSS) reception below the forest canopy, initial registration of the TLS project was performed in the project coordinate system. Additionally, the registered point clouds were cleaned from noisy points by removing points exceeding pulse deviation threshold (Wilkes et al., 2017).

2.3. UAV-LS protocol

All four study sites were flown with the same RIEGL RiCOPTER with VUX-1UAV UAV-LS system (Table 2). Typical air times were 20–30 min with 15–20 min mapping time per flight. Flights were planned with regularly spaced parallel flight lines across the target areas. At FG, an elaborate flight pattern design was tested: The first two flights were arranged to follow the directions of the plot boundaries, two more flights with a 45° rotation, and two more with the same direction as the first flight, but with modified scanner settings. At RC, the plot was located slightly beyond the maximum range of 500 m from the take off position, which resulted in limited coverage over the most southern part of the plot. Additionally, flight line spacing was wider than at NL and FG at 40 m to cover a larger area. At LF, one flight had to be flown manually due to an unsuccessful flight plan upload to the platform, resulting in an uneven distribution of flight lines. However, due to the open canopy structure at this savanna site canopy exploration was still very favourable for further analysis. Further details on the flight campaigns can be found in Table 1.

The UAV-LS processing followed standard procedures (Brede et al., 2017). First, the collected raw GNSS and IMU data were processed to flight trajectories with Applanix POSPac Mobile Mapping Suite 8.3 and under correction of GNSS logs received from permanent base stations. Second, LiDAR waveforms were processed to discrete return ranging data in the scanner's own coordinate system with RIEGL's RiPROCESS software. During this step all returns that would result in a reflectance of less than 20 dB were removed. Then, the trajectory in combination with

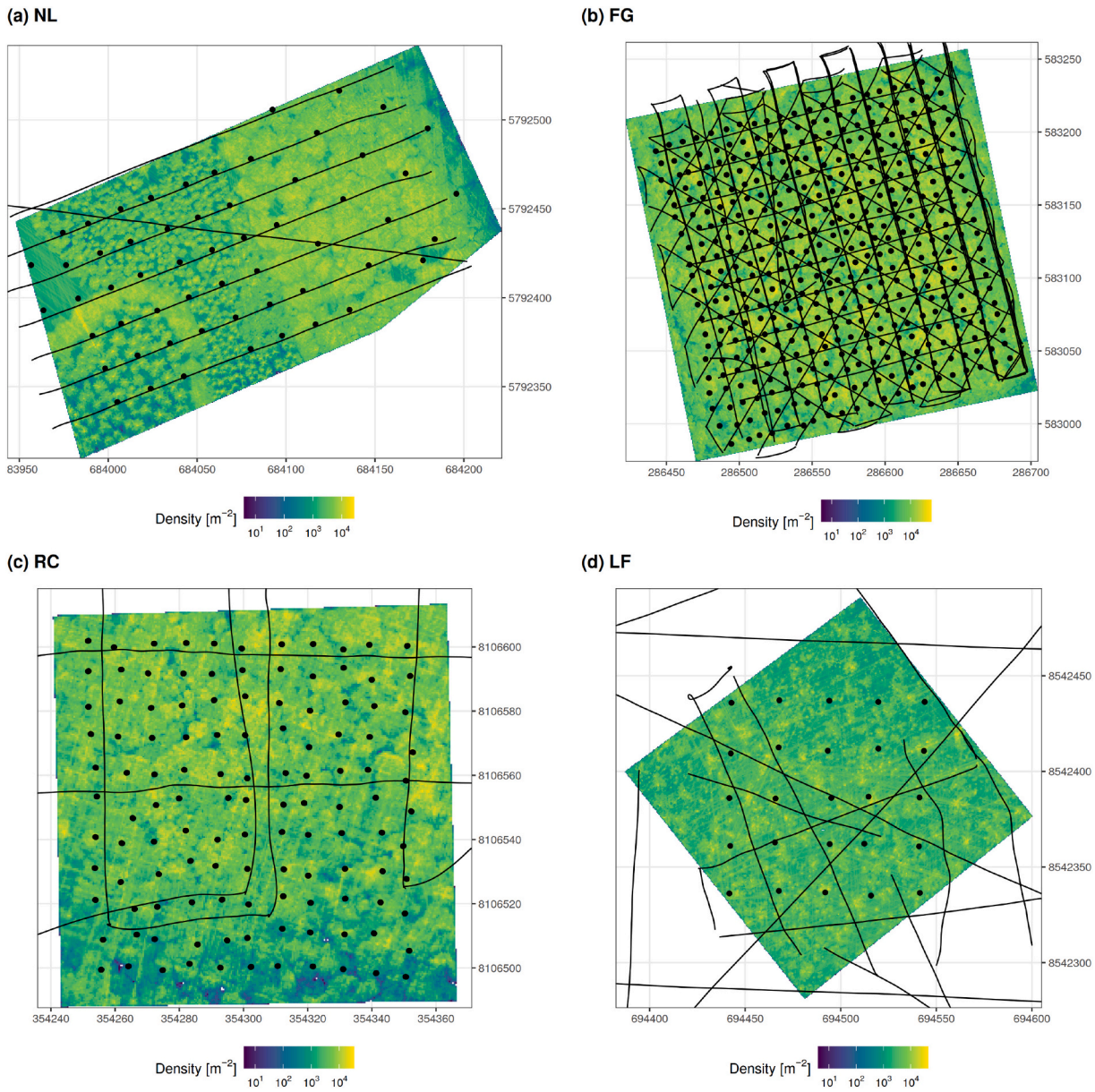

Fig. 3. UAV-LS point density maps of the involved sites. Black points indicate TLS scan positions and black lines UAV-LS flight lines. All geographic data are World Geodetic System 1984 WGS84 UTM. Universal Transverse MercatorUTM zones were 31N, 22S, 55N, 52N for NL, FG, RC and LF, respectively.

the laser ranging data was processed to point clouds on a flight line basis. Finally, flight line co-registration for each site was improved with RIEGL's RiPRECISION routine, which automatically searches for planar surfaces in the target area and uses them for fine-registration, similar to the MSA routine for TLS.

Three-dimensional registration of TLS with the UAV-LS point clouds was performed with manually selected registration targets with the alignment tool in CloudCompare v2.11 (https://www.danielgm.net/cc/). At the NL site, 12 registration targets (ground control points, GCPs) consisting of planar surfaces were used that were evenly spread over the site (Brede et al., 2017). At the FG and RC sites, no dedicated GCP were installed, because visibility could not be ensured from the UAV-LS. Therefore, branches of large trees, apex points of palms and terrain features, which were easy to identify in both TLS and UAV-LS point clouds, were used as targets. At the LF site, different objects on the scaffold tower in the centre of the site like guy-wire anchors and instrument mountings were used to co-register TLS and UAV-LS point clouds. Residual registration errors are listed in Table 1.

2.4. Wood density

Wood density estimates were retrieved from two global databases and a compilation study in order to estimate AGB based on individual tree volume estimates. Data for the NL temperate site were collected from the Wood Economics Spectrum database (Chave et al., 2009; Zanne et al., 2009), where data are stored as species level-averages. Since trees from the family *Fagaceae* could not be identified to the species level based on the UAV-LS data, they were summarised at the family level by averaging wood densities of the species *Fagus sylvatica*, *Quercus robur* and *Quercus petraea* (Table 3). All other species were treated with species-specific wood densities. Data for the tropical sites FG and LF were extracted from the Pantropical Tree Harvest database (Chave et al., 2014), where data are stored at single tree level. All available samples were averaged for French Guiana for the FG site, and for Australia for the LF site. Wood density representative of Australian wet tropical forests was taken from Bradford and Murphy (2019) for the RC site.

Table 1
Study site characteristics, TLS and UAV-LS campaign details.

	Speulderbos (NL)	Paracou (FG)	Robson Creek (RC)	Litchfield (LF)
Site characteristics & samples				
Biome	TBMF[a]	TMBF[b]	TMBF	TS[c]
Stem density [ha^{-1}]	204[d,e]	563[d]	967[d]	492[f]
Sampled area [ha]	1.8	4.0	1.0	1.0
Number of sampled trees [#]	199	171	192	310
DBH range of samples [cm][g]	8.9–94.3	8.0–158.8	16.4–195.1	5.1–56.9
Tree height range of samples [m][g]	9.0–36.4	10.4–44.6	18.5–37.4	5.4–24.8
TLS				
Grid spacing [m]	10 & 20	10	10	25
Scan positions [#]	58	441	121	50
UAV-LS				
Flights [#]	1	6	2	2
Flight height a.g.l. [m]	90	110	90	55
Flight speed [m s^{-1}]	6	6	2.5 & 8	6
Average point density [points/m^2]	3798	10090	4459	3744
TLS & UAV-LS				
Registration residual error [cm]	2.8	11.3	1.8	1.8

[a] Temperate broadleaf and mixed forest.
[b] Tropical moist broadleaf forest.
[c] Tropical savanna.
[d] DBH ≥10 cm.
[e] Density for beech and oak stand.
[f] DBH ≥5 cm, (Luck et al., 2020).
[g] Based on TLS point clouds.

Table 2
RIEGL VUX-1UAV and VZ-400 characteristics. The listed performance parameters correspond to the scan programmes used in the field campaigns at all sites.

Characteristic	VUX-1UAV	VZ-400
Pulse repetition rate (PRR) [kHz]	550	300
Effective measurement rate [kHz]	500	122
Maximum range [m]	340[a]	350[b]
Ranging accuracy & precision [mm]	10 & 5	5 & 3
Laser wavelength [nm]	1550	1550
Beam divergence [mrad]	0.5	0.35
Field of view [°]	330[c]	100 × 360[d]
Weight [kg]	4.3[e]	9.6[f]

[a] At target $\rho \geq 0.8$ and 550 kHz PRR.
[b] At target $\rho \geq 0.9$ and 300 kHz PRR (high speed mode).
[c] Across track.
[d] Zenith × azimuth.
[e] With inertial measurement unit (IMU).
[f] Without battery and tilt mount.

3. Methods

3.1. TLS trees and TLS tree metrics

For all four sites, sample trees were extracted from the TLS plot point cloud. These would serve as calibration for UAV-LS individual tree estimates. Individuals were sampled from across the plot area to capture different growing conditions within the plot as well as across tree sizes. Trees with DBH ≥ 5 cm as estimated in the TLS point clouds were primarily targeted. The largest trees within the plots were sampled with priority as they contain the bulk of plot AGB (Meyer et al., 2018). In this sense the sampling design was not random and did not represent the demography of trees, but aimed to capture largest contributors to the plot AGB. The largest trees were identified with help of the canopy height model models (CHMs), point cloud inspection and inventory stem maps, where available.

Table 3
Wood densities used to estimate AGB for the four sites.

Site	Taxonomic group	Wood density ρ [g cm^{-3}]	Source
NL	*Fagaceae*	0.568	Zanne et al. (2009)
NL	*Abies grandis*	0.350	Zanne et al. (2009)
NL	*Picea abies*	0.370	Zanne et al. (2009)
NL	*Pseudotsuga menziesii*	0.453	Zanne et al. (2009)
FG	Angiosperm (French Guiana)	0.626	Chave et al. (2014)
RC	Angiosperm (Australia, wet tropical)	0.630	Bradford and Murphy (2019)
LF	Angiosperm (Australia, general)	0.864	Chave et al. (2014)

At all sites, trees with trunks that bifurcated below 1.3 m were excluded from analysis. At the FG site, palms were not included in the sampling in line with Jucker et al. (2017). At the more open LF site, segmentation was less complicated and time-intensive due to rare crown overlap, so smaller trees were included in the sampling. In total, 199, 171, 191, and 310 trees were sampled at the NL, FG, RC and LF sites, respectively (Fig. 4 and Table 1). After selection, each sample tree was manually segmented from the TLS plot point cloud to ensure high segmentation quality. This included identification of the main trunk and branches, segmentation of the crown from neighbouring trees, removal of surrounding ground points and understorey, and removal of dead and tangled branches, lianas and epiphytes.

Subsequently, semi-automatic foliage segmentation was applied (Wang, 2020) with manual parameter tuning based on 10–20 trees per site and visual assessment. Finally, defoliated tree point clouds were used to build QSMs, and derive tree trunk and branch volume with *TreeQSM* v2.3. *TreeQSM* is a geometric fitting routine that models geometrically explicit trees by identifying the branching architecture, and fitting cylinders to represent trunks and branches (Raumonen et al., 2013). QSM-derived tree volume has been shown to be an unbiased predictor for individual tree AGB (Calders et al., 2015), especially for large trees (Gonzalez de Tanago et al., 2018; Momo Takoudjou et al., 2018). The latest version of *TreeQSM* is available at (https://github.com/InverseTampere/TreeQSM).

For automatic optimisation of *TreeQSM* parameters, a grid-search optimisation was applied on an individual tree basis. Specifically, for each parameter a vector of possible values was determined, then all possible parameter combinations were derived and *TreeQSM* was run 10 times for each combination. Then, the mean QSM to point cloud distance was computed for each QSM and averaged for all QSM of a parameter combination. The parameter combination with the smallest mean distance was identified as the best parameter combination for the particular tree. For this combination, *TreeQSM* was run again 25 times and the individual tree wood volume was calculated as the sum of the volume of all QSM cylinders. The repetition was applied to take into account the stochastic nature of *TreeQSM*. That is, *TreeQSM* contains a random component in the initiation stage of model fitting. This means for the same input parameters the resulting QSM will differ slightly from each other. Finally, the wood volume for a single tree was estimated as the mean across the 25 QSM.

In order to estimate individual tree AGB, the QSM tree volume was multiplied with the wood density corresponding to the tree's taxonomic group (Table 3). This approach assumes uniform wood density across the whole tree, while true wood density varies within a tree (Demol et al., 2021a) and within trees of the same species (Phillips et al., 2019). Intra-tree variations can even be systematic within functional groups,

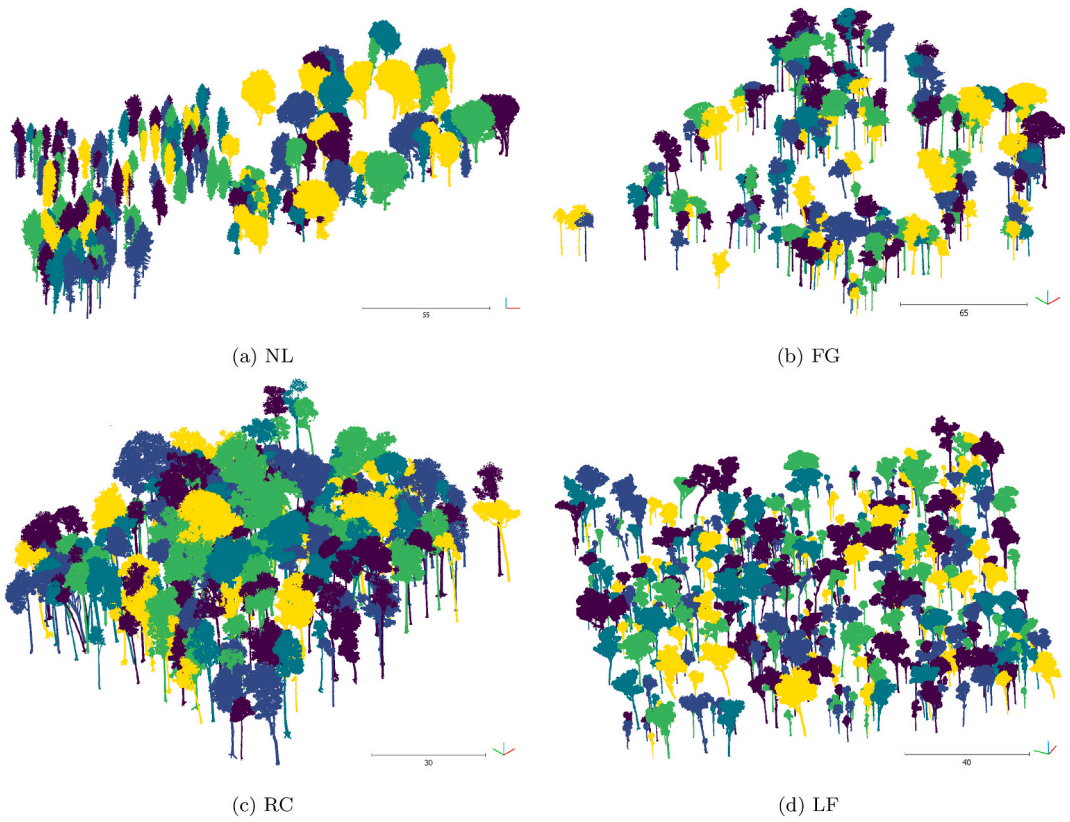

Fig. 4. TLS trees for involved sites. Individual trees are coloured for better visual interpretation.

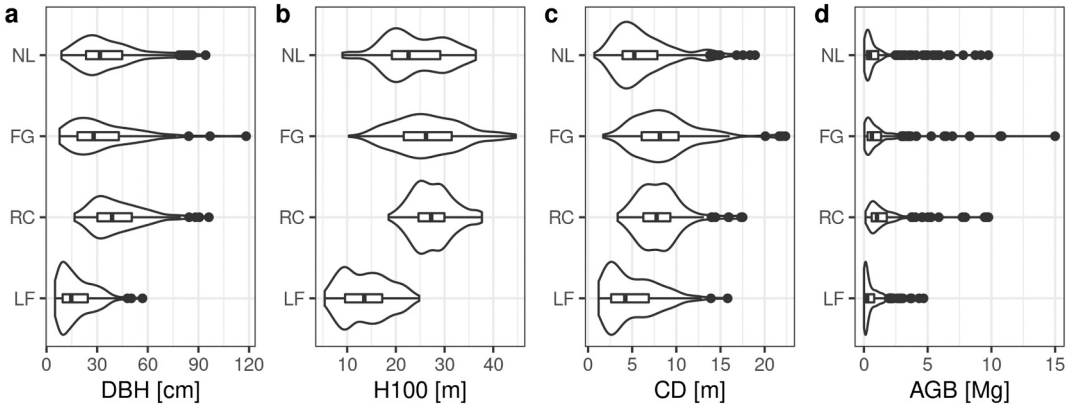

Fig. 5. TLS tree statistics across sites. (a) DBH based on least squares fitted cylinder fitted to TLS point cloud at 1.1–1.5 m above ground. (b) Tree height H100 based on difference between lowest and highest TLS point. (c) Crown diameter based on distance of convex hull centroid to convex hull vertexes. Convex hull derived from TLS point cloud. (d) AGB based on TLS QSM volume estimation and wood density (Section 3.1).

meaning that bias can propagate to stand level depending on the forest composition in pioneer species (Momo et al., 2020). However, volume-weighted wood density values are not widely available (Demol et al., 2021a), especially for tropical tree species.

Additionally to AGB, individual tree DBH was estimated as the diameter of the cylinder fitted to the height 1.1–1.5 m of the QSM at NL and LF. At FG and RC, where buttresses hampered this simple estimation procedure, a procedure based on the TLS point clouds was implemented that mimics field protocols for buttressed trees (Terryn et al., 2022): initially, a circle was fitted to a 6 cm thick point cloud slice at 1.3 m from the ground. If the average residual between the points and the fitted circle exceeded 0.001 times the fitted radius indicating a buttress, the process was repeated with the next point cloud slice 6 cm higher, until the criterion was met. The range between lowest and highest point in individual TLS tree point clouds was used as the TLS-based tree top height (H100).

3.2. *UAV-LS tree segmentation*

Automatic individual tree segmentation was performed with a recently developed method based on shortest paths (Raumonen et al., 2021). This method exploits the high density and explicit three-dimensional representation of trees within TLS and UAV-LS point clouds. The method first simplifies the point cloud by considering proximal points as patches. The patches together with their neighbours define a graph where the nodes are the centres of patches and the edges

are the lines connecting the neighbouring nodes. The method starts from the nodes below defined base height, and expands the shortest paths upwards into stems and branches. Due to occlusion the graph is incomplete such that some nodes and in particular edges are missing. To tackle this problem, the method defines the shortest paths iteratively: at each iteration the paths are expanded as far as possible with a restriction on path length to height ratio that relaxes at each iteration and thus can expand more horizontally into the branches. Then at each iteration, new connections from already connected nodes to unconnected nodes are created to complete the graph with likely connections. After the shortest paths have been defined, the trees are defined iteratively: First, select the node that has the most paths starting from it as this most certainly is on a large stem and select few layers of its neighbours as a section covering the stem. Now the tree is defined to consist of all those patches whose shortest paths end at this stem section. Then this process is repeated from the node that has the most paths starting from it and is not yet assigned to a tree. Finally, points in proximity to patch centres are assigned to the tree corresponding to the graph. Hence, the algorithm produces tree graph representations and individual tree point clouds. The method contains a set of parameters like initial thinning options, patch size and maximum allowed height to distance ratio. These parameters were manually tuned by comparing outputs with the TLS trees Appendix (A).

In order to link the UAV-LS segmented trees with the TLS trees (Section 3.1), the UAV-LS trees with the highest spatial overlap with the TLS had to be identified. For this purpose, for each TLS individual tree point cloud all UAV-LS point clouds were identified which had overlapping bounding boxes. Then, the TLS and all the UAV-LS individual tree point clouds were voxelised with a voxel side length of 0.25 m. Subsequently, the volume of the intersection and the union of the voxels sets, and the Jaccard index were calculated (Jaccard, 1912). The Jaccard index is a commonly used performance metric for semantic segmentation machine vision tasks and ranges from 0 (worst case) to 1 (best case). It has the advantage of taking into account both volume similarity as well as position in 3D space. The best matching UAV-LS individual tree point cloud was identified as the one with the highest Jaccard index (Figs. 6 and 7). This guaranteed that each TLS tree was matched with a UAV-LS, with varying levels of overlap quality. The Jaccard index is defined as:

$$J(T,U) = \frac{|T \bigcap U|}{|T \bigcup U|} \quad (1)$$

where T and U are the TLS and UAV-LS voxel sets, respectively, $|T \bigcap U|$ is the volume of their intersection, and $|T \bigcup U|$ the volume of their union.

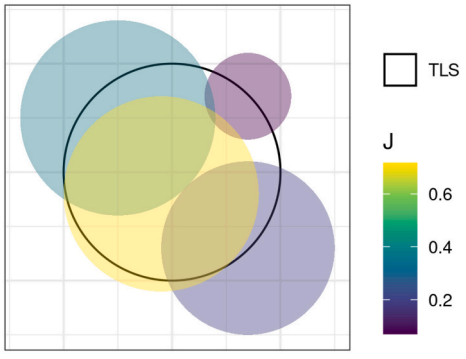

Fig. 6. Concept of the selection process of UAV-LS individual trees based on Jaccard index J in ground-projected view. Idealised UAV-LS trees as filled and TLS trees as black outlined circles. The UAV-LS tree with the highest J is chosen as the representative for the TLS tree.

3.3. UAV-LS tree metrics

A range of metrics was derived from UAV-LS individual tree point clouds. In particular, the H100 was estimated as the difference between highest point and the digital elevation model (DEM) derived from UAV-LS. Tree height is commonly used in ASM based on field inventories (Chave et al., 2005, 2014). Additionally, the 95th percentile H95 and the median height above ground of all points H50 were calculated. Using the 95th percentile instead of the H100 aims to reduce the influence of spurious noise in the points clouds. H50 can be regarded as a discrete return equivalent to the height of median energy (HOME) metric based on full-waveform LiDAR, which has been shown to be well correlated with plot AGB (Drake et al., 2002). Tree height is correlated to AGB, in particular when trees across age classes are compared (Dalponte and Coomes, 2016; Asner and Mascaro, 2014), but saturates with tree age and high plot AGB. As height metrics can be very reliably derived from ALS, UAV-LS and space-borne LiDAR data, they are important for remote sensing-based approaches (Jucker et al., 2017; Dalponte and Coomes, 2016; Brede et al., 2017; de Oliveira et al., 2021; Liu et al., 2018; Duncanson et al., 2022).

Another category of derived metrics was related to crown dimensions. For this purpose the crown was modelled as the convex hull derived from the ground-projected tree points (Dalponte and Coomes, 2016). This assumed that the crown points define the maximum ground-projected extent of the individual tree point cloud. Subsequently, crown area (CA) and crown perimeter (CP) were defined as the area and the perimeter length of the convex hull, respectively. For the estimation of crown diameter (CD) in a way comparable to field measurements, the position of the trunk was estimated as the centroid of the convex hull. Then the distance of the centroid to the convex hull edge in the four cardinal directions was derived and the CD was derived as the average of these four distances multiplied by two. Crown dimensions have been identified as unbiased predictors of AGB across tropical field plots (Meyer et al., 2018).

Furthermore, the volume that a tree occupies within the forest canopy was defined as the volume inside the alpha hull derived from the individual tree point cloud with parameter $\alpha = 1$ m (V). This metric should not be confused with the accumulative branch volume derived from TLS QSM. This metric follows the rationale that larger trees containing more AGB need to occupy more canopy volume. The tree occupied volume is difficult to derive from low density ALS point clouds, which cannot depict the typology of the tree in complex canopies. Alpha shapes have been used to characterise the volume that a tree occupies in the canopy volume with TLS point clouds (van der Zee et al., 2021).

The individual tree graphs that were produced during the individual tree segmentation (Section 3.2) were utilised for tree metric estimation (Fig. 8). For this purpose the graphs were interpreted as pseudo trees that do not reproduce the tree structure in terms of volume, but in terms of topology. Specifically, the total graph edge length (GEL) was derived as a sum of cumulative edge lengths, which are the distances of a node to the tree root node, and the graph nodes (GN) was the total number of nodes in a graph. Graph based tree metrics have not been explored yet for AGB estimation.

Finally, the two compound variables H100 $\times$ CD (HCD) (Jucker et al., 2017) and GEL $\times$ CD (GELCD) were derived.

In a first step to understand the agreement between UAV-LS and TLS, the two metrics H100 and CD, which are two widely used metrics of ASMs due to the possibility to measure them in the field, were directly compared. For this H100 and CD were estimated from the TLS point clouds in the same way as for UAV-LS. Furthermore, UAV-LS metrics were individually compared to TLS QSM estimated tree wood volume to get insights in the potential of the metrics to estimate wood volume in modelling. For this purpose linear relationships in linear space, i.e., not log-transformed, were used. The idea behind this was to use the same relationship for all metrics. A linear relationship in linear space would also be the most desirable for calibration purposes because linear

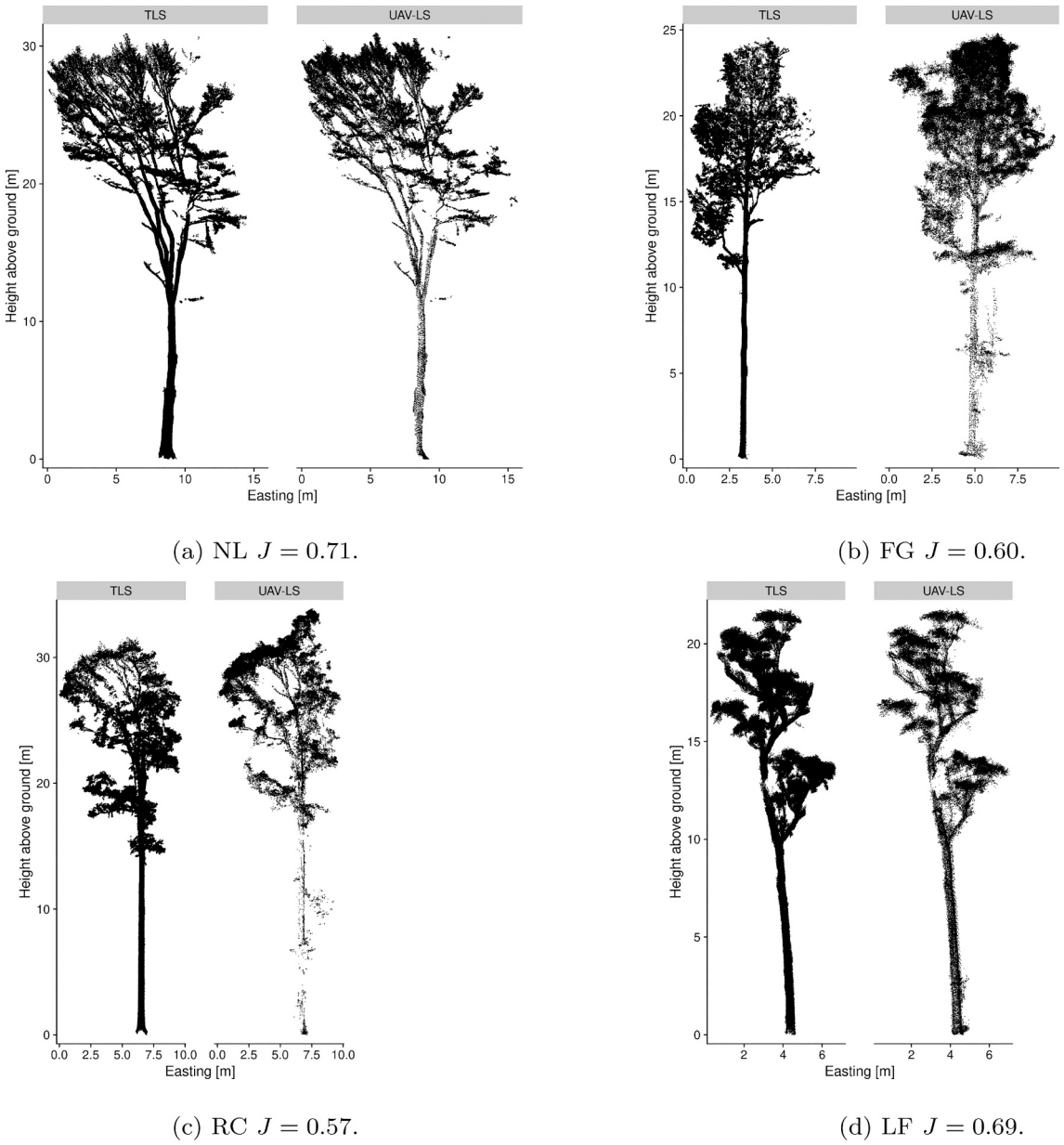

Fig. 7. Best segmented individual tree point clouds. Only 2 m deep slices centred on the trunk are displayed. Jaccard index J of segmentation in sub-caption.

relationships need a small number of samples for calibration when compared to log-transformed data.

3.4. Individual tree AGB modelling strategies

Different AGB modelling strategies were tested depending on the scenarios of available input data: field-measured metrics, i.e., DBH, CD and height, TLS and UAV-LS surveys, and their combinations (Table 4). Two broad modelling categories were distinguished: on the one hand, models that are calibrated off-site, i.e., with trees sampled in the same biome but not at the specific site, labelled as global strategies. These models need to be found in relevant publications or can be calibrated based on published data. On the other hand, models that are calibrated with local, non-destructively sampled trees, were labelled as local strategies. All of these models relied on TLS QSM estimated AGB and therefore were subject to errors in these estimates.

3.4.1. Strategy Ia: globally calibrated inventory-based ASM

Strategy Ia aimed to cover situations where local calibration data were absent and forest inventory techniques would be used to scale the model across the reference site. It involved the collection of traditionally measured inventory data required by the respective ASM and the application with a published model. As no ASM calibration was necessary, all TLS trees were used for validation. For the NL site the ASM of Forrester et al. (2017) was adopted:

$$\mathrm{AGB} = \exp(\ln(\beta_0) + \beta_1 \ln(D)) \times \mathrm{CF} \quad (2)$$

with *AGB* in kg, *D* is DBH in cm based on TLS, and β_0, β_1 and *CF* species specific correction coefficients. Species-specific coefficients were used for *Picea abies* and *Pseudotsuga menziesii*, while the coefficients for *Abies alba* and broad-leaf were used for *Abis grandis* and *Fagaceae*, respectively (Table 5).

For all the other sites, the pan-tropical ASM of Chave et al. (2014) was used:

$$\mathrm{AGB} = 0.0673 \times (\rho D^2 H)^{0.976} \quad (3)$$

with *AGB* in kg, ρ is wood density in g cm^{-3}, *D* is DBH in cm, H100 is tree

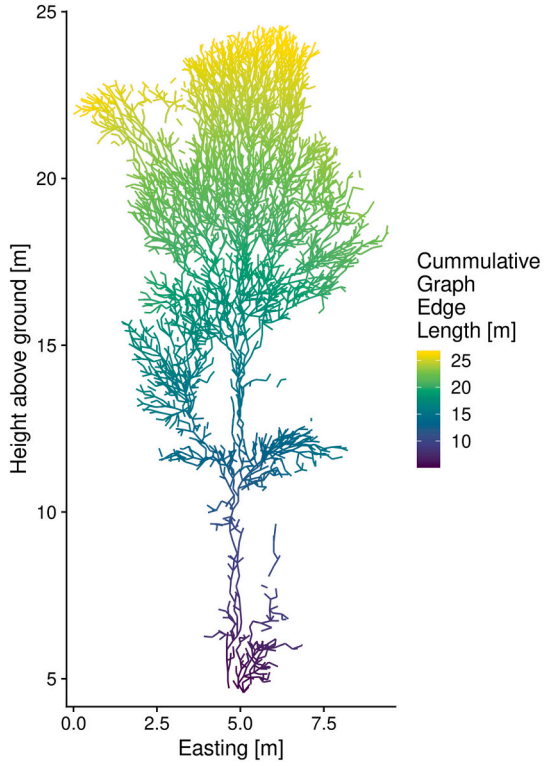

Fig. 8. Slice through sample graph width 2 m depth. Cumulative edge lengths are the distances of node to the tree root node.

Table 4
AGB modelling strategies of this study. Local and global refer to the scope of the calibration data, where local means data exclusively from plot and global means data from other places. Inventory-based refers to measurements that are possible with traditional inventory methods, such as DBH and tree height. Scaling refers to the technology used for application at reference sites.

Strategy	Calibration	Involved metrics	Validation approach	Scaling
Ia	Inventory-based global	DBH, H100[a]	All samples for validation	inventory
Ib	Inventory-based global	H100, CD	All samples for validation	UAV-LS
IIa	TLS local	DBH, H100	LOOCV	Inventory
IIb	TLS local	H100, CD	LOOCV	UAV-LS
IIc	TLS local	All[b]	LOOCV	UAV-LS

[a] H100 not used at site NL.
[b] H100, H95, H50, CA, CD, CP, V, GN, GEL, HCD, GELCD, Taxonomy (only NL).

Table 5
ASM coefficients used for modelling strategy Ia based on Forrester et al. (2017).

Species/Taxonomic group	$ln(\beta_0)$	β_1	CF
Picea abies	−1.887	2.303	1.059
Pseudotsuga menziesii	−2.330	2.482	1.003
Abies grandis	−2.396	2.450	1.001
Fagaceae	−1.996	2.363	0.997

height in m. DBH and H100 estimates of TLS were used.

3.4.2. Strategy Ib: globally calibrated UAV-LS-based ASM

Strategy Ib was similar to strategy Ia in the sense that a calibrated ASM was used. In this case, this ASM was built on metrics that are possible to measure from ALS and UAV-LS, hence, scaling of AGB estimates would be possible with airborne LiDAR technology. Jucker et al. (2017) presented an ASM trained on a global database of inventory measured individual tree metrics and destructive harvest-derived AGB of 2395 trees. The proposed ASM was built on the metrics tree height H100 and crown diameter CD. The model differentiates angiosperm and gymnosperm species due to their structural differences:

$$\mathrm{AGB} = (0.016 \times \alpha_G) \times (H \times \mathrm{CD})^{2.013+\beta_G} \times 1.021026 \quad (4)$$

with *AGB* in kg, H100 and CD in m, and $\alpha_G = 0.093$ and $\beta_G = -0.223$ for gymnosperms, with both parameters set to zero for angiosperms.

3.4.3. Strategy IIa: locally calibrated inventory-based ASM

Strategy IIa simulated the use of locally collected TLS data for non-destructive calibration and inventory-based application. This approach was previously proposed by studies that employed TLS for direct AGB estimation (Calders et al., 2015; Momo Takoudjou et al., 2018; Lau et al., 2019). The strategy assumed the scanning of a reasonably large number of sample trees, which can be achieved by area-based scanning of established plots. The application at the hectare scale would then be achieved with traditional field inventories. The general ASM form of Chave et al. (2014) was adopted, calibrated with the TLS trees for each site individually and data were binned in log-transformed *D* (Duncanson et al., 2015; Jucker et al., 2017):

$$\ln(\mathrm{AGB}) = \alpha + \beta \ln(\rho D^2 H) + \varepsilon \quad (5)$$

with individual tree *AGB* based on TLS estimates in kg, ρ is the wood density in g cm^{-3} (Table 3), *D* is the DBH in cm, H100 is tree height in m as derived from the TLS point cloud. In order to retransform the data to linear units a correction factor $CF = exp(RSE^2/2)$ was applied as proposed by Baskerville (1972).

3.4.4. Strategy IIb: locally calibrated UAV-LS-based ASM

Strategy IIb used a per-site calibrated ASM based on H100 and CD that can be extracted from ALS and UAV-LS. This strategy assumed the presence of TLS and UAV-LS data for the same site, with synchronised scanning campaigns. The general ASM form of Jucker et al. (2017) was used and as in strategy IIa models were fitted on log-transformed, binned data:

$$\ln(\mathrm{AGB}) = \alpha + \beta \ln(H \times \mathrm{CD}) \quad (6)$$

with *AGB* in kg, H100 and CD in m, and α and β model coefficients that were fitted separately for angiosperm and gymnosperm species (Jucker et al., 2017).

3.4.5. Strategy IIc: locally calibrated UAV-LS-based non-parametric model

Strategy IIc assumed the same conditions as strategy IIb, i.e., availability of TLS and UAV-LS data, but strategy IIc made use of a wider range of UAV-LS based metrics and a non-parametric modelling approach. In particular, all metrics presented in Section 3.3 plus taxonomic information, i.e., coniferous vs deciduous species, were considered for the modelling process to build local AGB prediction models for UAV-LS data. The rationale behind the use of multiple metrics was to possibly mitigate errors in retrieval of single metrics and optimise the prediction power of individual metrics in different forest structures.

The non-parametric modelling approach adopted was random forest (RF) for regression (Breiman, 2001) implemented in the R `ranger` package (Wright and Ziegler, 2017). RF has gained popularity in remote sensing applications because of its robustness to multi-dimensional and co-linear data (Belgiu and Drăgu, 2016).

In this study, RF was trained to predict individual tree volume based on all available tree metrics (Section 3.3). Subsequently, volume was multiplied with wood density to derive AGB based on the same species information as for the TLS estimates (Sections 2.4, 3.1). Hyper-parameter tuning via cross-validation showed low sensitivity to hyper-

parameter choices in terms of volume prediction performance root mean square error (RMSE). Therefore, default values were implemented: number of regression trees to grow of 500, minimal node size of 5 and number of metrics to possibly split at in each node of 3.

Additionally, the RF importance metrics were analysed in order to gain understanding in the relative importance of metrics within and across sites. For this purpose, importance metrics were extracted from each trained RF during leave one out cross validation (LOOCV) and the scores were averaged within the site. Finally, importance scores were normalised by division by the highest score per site to make the sites inter-comparable.

3.5. Error assessment

As stated in the description of the strategies, strategies Ia and Ib, which implemented calibrated ASMs, could use all TLS trees for independent validation, while strategies IIa, IIb and IIc implemented LOOCV to make best use of the available TLS trees for training and validation, and to get insight into model performance on unseen samples. Error metrics were derived independently for each site and then compared across sites. The error metrics that were derived for individual tree AGB prediction were the RMSE in Mg and the relative root mean square error rRMSE in %:

$$\mathrm{RMSE} = \sqrt{\frac{1}{N}\sum_{i=1}^{N}\left(\mathrm{AGB}_i^{\mathrm{TLS}} - \widehat{\mathrm{AGB}}_i\right)^2} \tag{7}$$

$$\mathrm{rRMSE} = \frac{\mathrm{RMSE}}{\frac{\sum_i^N \mathrm{AGB}_i^{\mathrm{TLS}}}{N}} \div 100 \tag{8}$$

with $\mathrm{AGB}_i^{\mathrm{TLS}}$ and $\widehat{\mathrm{AGB}}_i$ the TLS estimated and modelled AGB of the i^{th} tree, respectively. It should be noted that this is not an RMSE based on log-transformed AGB but on natural scale. Log-transformation is regularly applied to AGB data for use in linear statistics (Picard et al., 2012), but residual errors are not intuitive to understand in log-space and cannot be compared across tree sizes. Natural instead of log-transformed units are more intuitive for understanding of the error and to be able to sum up individual errors across tree sizes. Additionally, satellite mission requirements are formulated in natural scale, so that a formulation of individual tree errors in natural scale is more useful.

Furthermore, absolute and relative biases of the cumulative population AGB were calculated in order to get an understanding of the individual models' ability to produce an accurate estimate for each site when all trees' AGB is counted together as would be the case for satellite calibration and validation. The absolute bias was derived to get an understanding of the performance with respect to satellite mission requirements, while the relative bias was used to compare across sites with different AGB stocks:

$$\mathrm{Bias}_{\mathrm{absolute}} = \sum_i^N \widehat{\mathrm{AGB}}_i - \sum_i^N \mathrm{AGB}_i^{\mathrm{TLS}} \tag{9}$$

$$\mathrm{Bias}_{\mathrm{relative}} = \frac{\sum_i^N \widehat{\mathrm{AGB}}_i - \sum_i^N \mathrm{AGB}_i^{\mathrm{TLS}}}{\sum_i^N \mathrm{AGB}_i^{\mathrm{TLS}}} \times 100 \tag{10}$$

with $\mathrm{AGB}_i^{\mathrm{TLS}}$ and $\widehat{\mathrm{AGB}}_i$ the TLS estimated and modelled AGB of the i^{th} tree, respectively, and $Bias_{absolute}$ in Mg and $Bias_{relative}$ in %. According to these definitions a positive bias means overestimation. It should also be noted that these definitions differ from those of Chave et al. (2014) and Jucker et al. (2017), who focus on individual tree bias assessment.

3.6. Impact of calibration sample size on AGB prediction

The collection of calibration data with TLS in the field (Wilkes et al., 2017) and subsequent manual preparation of TLS trees are time consuming procedures. Therefore, the effect of the calibration sample size on the prediction errors was analysed for locally calibrated strategies IIa, IIb and IIc, and independently for each site. This was achieved by varying the number of the samples available for model calibration.

Specifically, for each individual tree in the TLS database a stratified random sample of n samples was drawn from the remaining trees, whereby n was varied from 10 to the maximum available number of TLS trees minus the tree for prediction per site in steps of five. In this way predictions were always performed on all individual trees, while the number of calibration samples was varied according to n. The stratification was implemented with five strata and based on total QSM wood volume. The rationale behind the stratification is that when selecting calibration samples in the field, field crews would be able to distinguish five size classes of trees according to their height and DBH as proxies for total tree wood volume, and with knowledge of the range of tree sizes in the area. Additionally, stratification is recommended for ASM model calibration (Jucker et al., 2017; Duncanson et al., 2015).

For the NL site, where taxonomic groups were distinguished in strategy IIa and IIb (Section 3.4), the calibration models were built independently for the taxonomic groups. For this case, the number of randomly drawn samples was proportionate to the proportion of the respective taxonomic group in the full TLS database. This effectively increased the number of samples n needed in the sampled database to built models for the site, so that at least 25 and 50 samples were necessary for strategy IIa and IIb, respectively.

Based on the resulting calibration database a model according to strategies IIa, IIb and IIc was built (Section 3.4), and the individual tree AGB was estimated. Then, RMSE (Eq. (7)) and relative bias (Eq. (10)) were calculated. Subsequently, this procedure was applied to all individual trees for a given sample size n. The procedure was repeated 20 times, and the mean and standard deviation of RMSE (Eq. (7)) and relative bias (Eq. (10)) were calculated. The resulting statistics enabled assessment of the performance of the modelling strategies under different sizes for the calibration database.

4. Results

4.1. TLS and UAV-LS H100 and CD comparison

The individual tree metrics H100 and CD showed generally good agreement between TLS and UAV-LS with $R^2 \geq 0.71$ for all sites except RC (Fig. 9). Tree heights achieved larger R^2 than CD across all sites, showing higher agreement in tree height than in CD. On average, UAV-LS trees were 1.00 m higher than TLS trees, reflecting a commonly observed difference of TLS and ALS that is due to occlusion of tree tops when observed from the ground (Hilker et al., 2010; Brede et al., 2017). For both metrics, strong differences in agreement occurred across sites. On the one hand, H100 and CD were strongly related at LF with R^2 of 0.99 and 0.92, respectively. The openness of the savanna woodland meant good detection of the ground and delineation of crowns from UAV-LS. On the other hand, at RC the delineation of the crowns was challenging due to a dense canopy and occurrence of lianas. However, it was evident that the tallest trees agreed strongly between TLS and UAV-LS across all sites, also reflected in general good segmentation as expressed by J (Fig. 9). The tallest trees were typically emergent trees that are clearly recognisable from on top of the canopy, and that can be characterised even in structurally complex forests and with lower requirements on the point cloud density (Meyer et al., 2018).

4.2. Relationships of individual metrics with tree volume

The explored TLS and UAV-LS metrics showed linear and non-linear relationships with QSM wood volume, and explained 19–88% of the variance in volume when assuming linear relationships (Fig. 10). Between sites the explained variances varied strongly with average

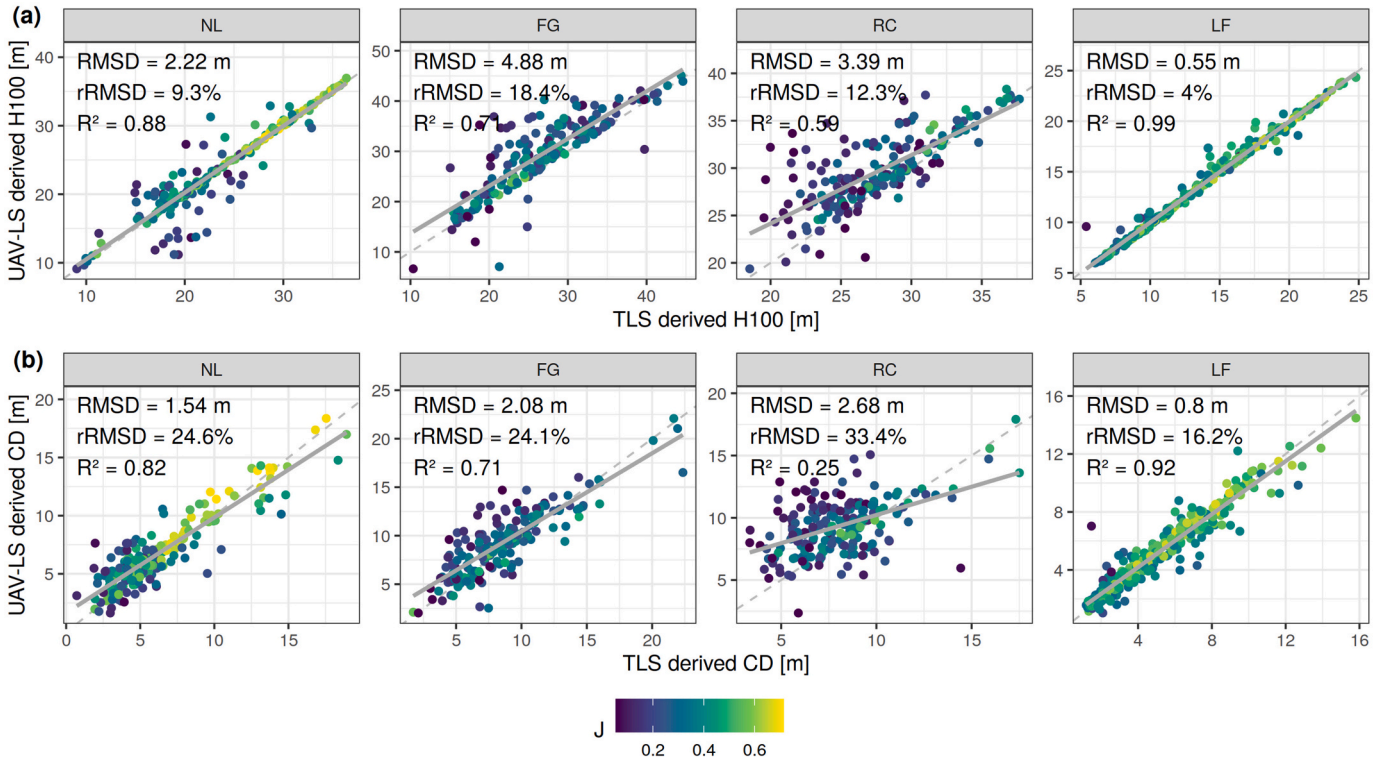

Fig. 9. Comparison of TLS and UAV-LS derived tree metrics (a) tree top height H100 and (b) crown diameter (CD) across all sites. RMSD refers to the root mean square difference (RMSD) between TLS and UAV-LS metrics. Grey solid lines indicate least squares fitted linear trends. Grey dashed lines indicate 1:1 lines. Points coloured according to their Jaccard index *J* of the UAV-LS tree with its respective TLS tree.

explained variance of 67, 49, 26, 71% for NL, FG, RC, and LF, respectively. This gradient reflects the varying structural complexities of the sites. Additionally, when comparing FG and RC, the lower UAV-LS point cloud density negatively affected the segmentation quality and hence robust estimation of metrics at RC. However, in order to solely focus on effects of point cloud density, a thinning experiment would need to be performed for each site.

DBH was overall a good predictor of tree wood volume with 83, 77, 73, 74% of variance explained at NL, FG, RC and LF, respectively. At NL, DBH was clearly non-linearly related to total tree wood volume, but showed low heteroscedasticity. At FG, RC and LF the non-linearity was less pronounced, but residuals had larger variance at high volume, making the relationship less suitable for modelling.

Height-related metrics estimated with UAV-LS were typically robust predictors of wood volume for small trees, but showed large residual variance for large trees. For the closed canopies of NL and FG the explanatory power of H50 was higher compared to the tree top height H100 with $R^2 = 0.23$ and 0.30 for H100 for NL and FG, respectively, and H50 with $R^2 = 0.25$ and 0.38 for NL and FG, respectively (Table 6). At the open Savanna site LF, H100 was more powerful ($R^2 = 0.62$) compared to H50 ($R^2 = 0.53$). At NL an impact of species on the height-volume relationship was clearly noticeable with angiosperm species strongly deviating from gymnosperm species (Fig. 10), making it necessary to take species into account for volume modelling.

Crown related metrics based on UAV-LS were generally well correlated with volume explaining up to 88, 64, 29, 82% of the variance in volume for NL, FG, RC and LF, respectively. In particular CA showed strong linear relationships, which let it be the best linearly correlated variable with volume in NL and FG with 88 and 64% of explained variance, respectively. Additionally, CA appeared to be more linearly related to tree wood volume than CD.

Both alpha hull-based tree volume *V* and graph related metrics showed strong linear relationships with wood volume with explained variance of up to 88%. Furthermore, no asymptotic behaviour could be observed at high wood volume. However, variance was not constant with higher variance of tree volume and graph metrics for higher wood volumes (Fig. 10).

Table 6
R^2 between individual tree metrics and TLS QSM derived individual tree volume across sites. DBH derived from TLS and all other metrics from UAV-LS. graph nodes (GN), GEL×CD (GELCD), H100×CD (HCD).

Metric	NL	FG	RC	LF
DBH	0.83	0.77	0.73	0.74
H100	0.23	0.30	0.27	0.62
H95	0.23	0.34	0.19	0.58
H50	0.25	0.38	0.22	0.53
CA	0.88	0.64	0.22	0.77
CD	0.77	0.50	0.19	0.69
CP	0.78	0.48	0.17	0.69
V	0.86	0.48	0.29	0.82
GN	0.87	0.50	0.31	0.81
GEL	0.87	0.58	0.39	0.82
HCD	0.72	0.55	0.31	0.78
GELCD	0.82	0.62	0.41	0.76

4.3. Individual tree AGB estimation

Individual tree AGB prediction accuracy varied both between sites and modelling strategies (Figs. 11 and 12). The AGB modelling strategy with the lowest RMSE across sites was strategy IIa with RMSE of 0.43, 0.54, 0.69, 0.30 Mg for NL, FG and RC and LF, respectively.

The two strategies Ia and Ib that rely on externally calibrated ASM showed strong linear trends between TLS estimated and predicted AGB, but with strong over- or underestimation at high AGB. In particular, strategy Ib generally overestimated gymnosperm species' AGB at NL, while angiosperm species were underestimated for trees with AGB $\geq$ 2.5 Mg at RC and LF. This could be explained by the calibration being

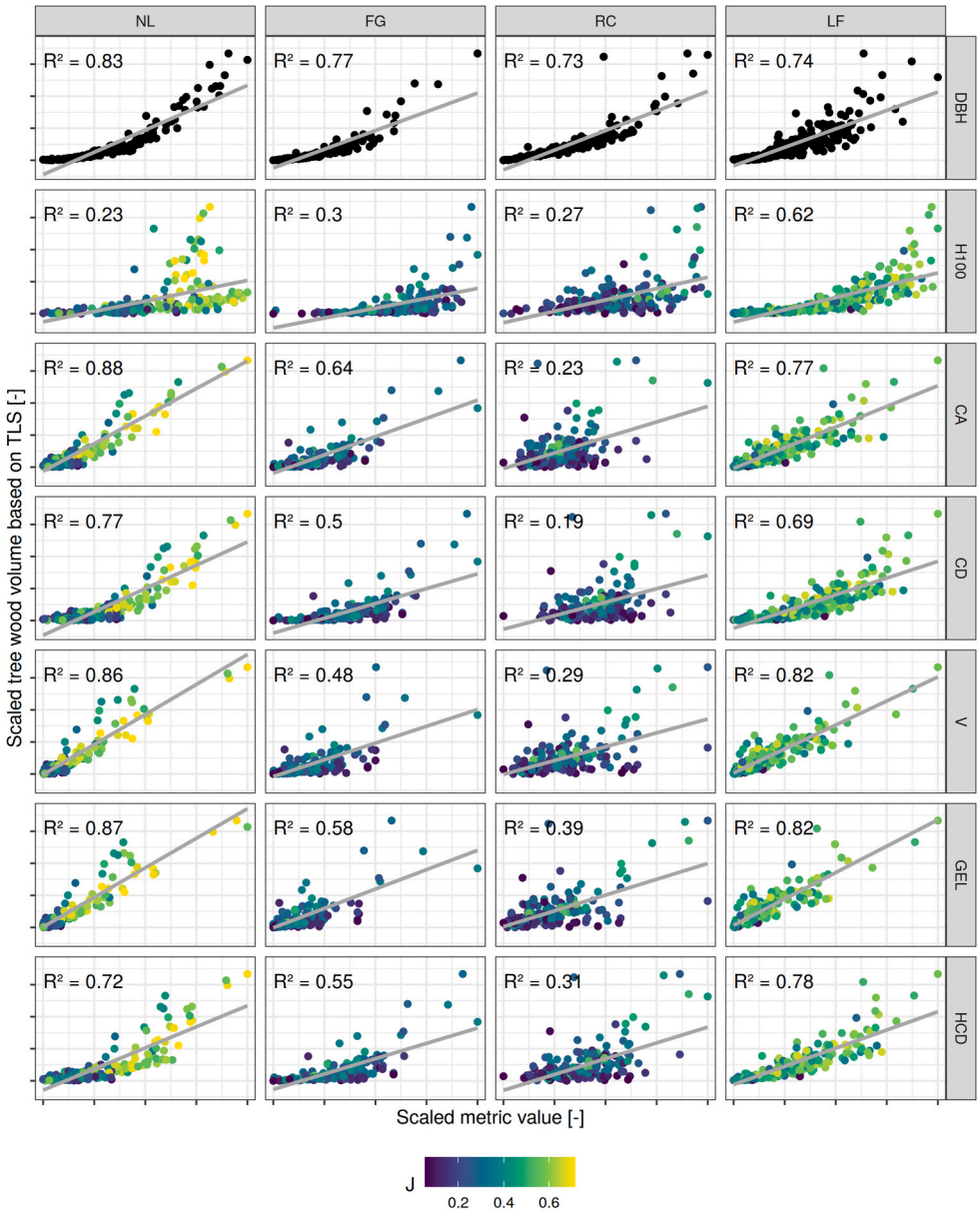

Fig. 10. Relationship of selected individual tree metrics (*x*-axis) with TLS derived tree volume estimation (*y*-axis). Vertical panels represent different UAV-LS metrics. Horizontal panels represent the sites. All metrics have been scaled between 0 and 1, and axis labels have been omitted to improve readability. Grey, dashed lines connects the minimum and maximum observed axis values in scaled space. R^2 correspond to coefficients of determination of the linear relationships. Points coloured according to their Jaccard index *J* of the UAV-LS tree with its respective TLS tree, except for DBH, which was derived from manually segmented TLS.

done on harvest trees not representative for the area or the calibration containing harvest samples from larger areas (e.g., Chave et al., 2014). Additionally, the calibration was performed on inventory measured metrics, while the ASM were applied on TLS and UAV-LS estimated metrics. Especially metrics like individual tree top height H100 is difficult to measure correctly in closed canopies (Wang et al., 2019).

The two strategies IIb and IIc relying on both available TLS and UAV-LS data showed small differences with each other, with strategy IIc having smaller RMSE of 0.01, 0.05, 0.29 Mg at NL, FG and RC, respectively, and no difference at LF (Fig. 12).

The RF non-parametric model provided additional information on the importance of individual UAV-LS metrics (Fig. 13). Generally, metric importance varied strongly across sites with few metrics scoring high importance or dominating at more than two sites, indicating a strong interplay of metrics. Only graph-based GEL and compound metric GELCD showed relative importance $\geq$0.9 at three and two sites, respectively. Field-inventory metrics were generally less important with relative importance $\leq$0.9, with the exception of H100 at RC. Taxonomic information (angiosperm vs gymnosperm species) was only included at NL and showed low importance. This might be explained by the good correlation of the UAV-LS metrics with AGB across species (Fig. 10).

4.4. Impact of calibration sample size on AGB prediction

When comparing the different AGB modelling strategies that were based on local calibration, strategy IIa consistently provided the lowest RMSE of all strategies across sites with on average 0.42, 0.56, 0.70, 0.30 Mg for $n \geq 50$ for NL, FG, RC and LF, respectively (Fig. 14). Moreover, there were no significant trends with changing TLS database size for $n \geq 50$. Since strategy IIa was the only one involving DBH as an independent variable, this result highlights the importance of DBH in AGB estimation of single trees.

Strategies IIb and IIc showed comparable, decreasing trends in RMSE with n at NL and FG, and divergent trends at RC and LF. Specifically, the RMSE of strategy IIb increased monotonically with increasing n from 1.38 Mg ($n = 30$) to 1.79 Mg ($n = 180$) at RC, and with $n \geq 100$ at LF. The very pronounced RMSE increase at RC might be explained with the growing number of small trees that get included in the calibration

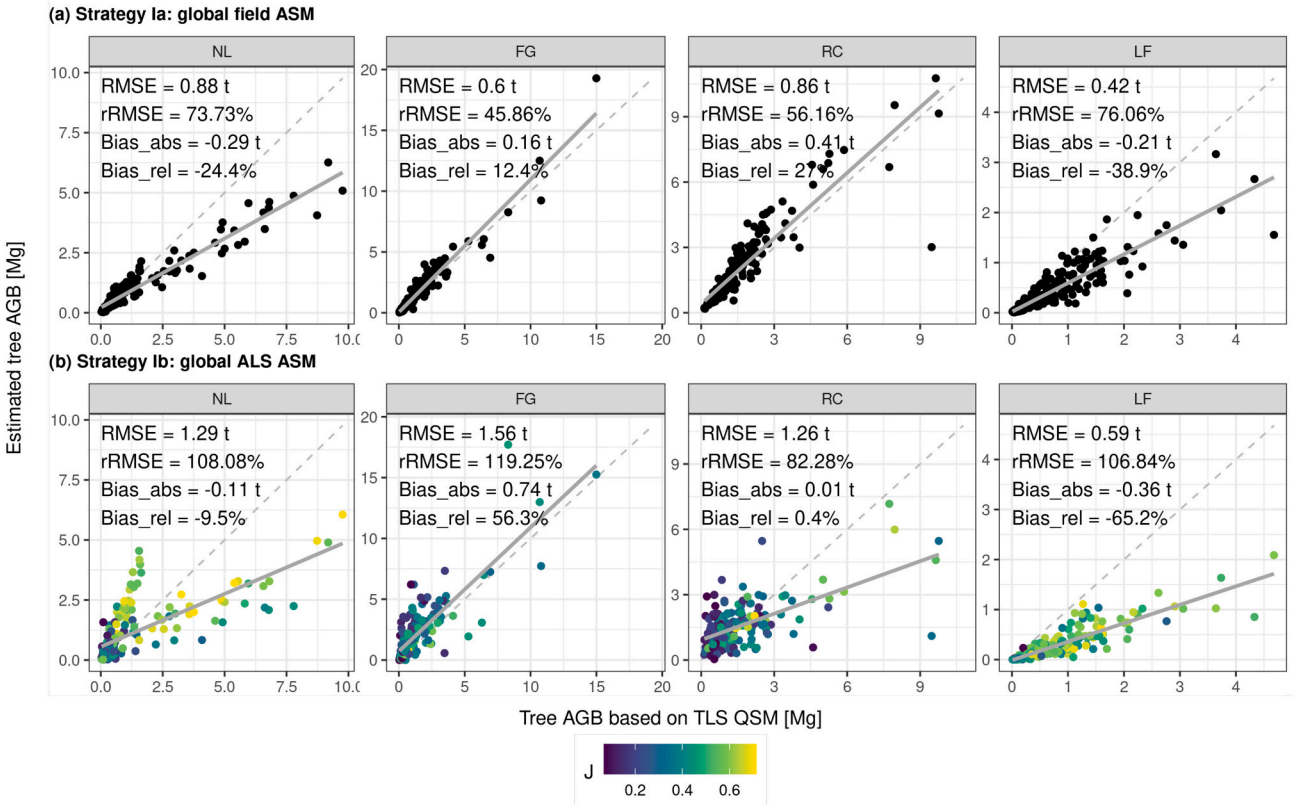

Fig. 11. Individual tree AGB estimation with modelling strategies based on globally calibrated ASM. Points coloured according to their Jaccard index *J* of the UAV-LS tree with its respective TLS tree. Grey dashed lines indicate 1:1 lines. Solid grey solid lines are linear trend models.

database. The stratified sampling approach implemented in the drawing produced relatively balanced calibration databases at small *n*, but due to the abundance of small trees (Fig. 5) more and more small trees were included with increasing *n*, and dominated the calibration. Particularly at RC, where the UAV-LS point density was low compared to the other dense tropical site FG (Table 1 and Fig. 3), the segmentation quality for small understorey trees was lower, which negatively affected the model calibration.

The results in terms of relative bias showed a different picture than the individual tree RMSE results. For strategies IIa and IIb, the largest possible TLS database did not result in the bias closest to 0%. In fact, for strategy IIa optimal *n* in terms of bias was 50, 85, 150 and 65 for NL, FG, RC and LF, respectively.

Strategy IIb showed different behaviours of relative bias at the four sites. At NL, bias monotonically decreased with bias closest to 0% of 0.02% at 80 samples. At FG, RC and LF monotonic increases in bias were observed. At FG, bias for $n = 20$ was 3.05% compared to 12.60% with 120 samples. At RC and LF the relative bias monotonically increased with *n*, resulting in heavily biased models peaking at 20.20, 14.40% at RC and LF, respectively.

Contrary to the differing trends between sites of strategies IIa and IIb, strategy IIc showed similar trends of bias across sites with biases of −9.54, −12.27, −7.02, and −8.70% at $n = 10$ indicating underestimation. With more than 25, 55, 15, and 30 samples available at NL, FG, RC and LF, respectively, the absolute bias dropped below 5%. When comparing strategy IIa and IIc based on RMSE and relative bias results, it became clear that strategy IIa provided the better individual tree AGB estimate but strategy IIc the better estimate of the cumulative AGB of a population of trees. This indicates that the non-parametric models in strategy IIc produced higher variance in the prediction of individual trees but that these prediction errors even out much more during summation. This can be explained with the modelling approach of RF, which basically fits many linear models and their predictions are weighted according to where in the features space the given observations are located. In practice, this provides a flexible model that adjusts to the provided observations. This non-linear behaviour plus the reliable trend of the bias towards 0% with increasing *n* are favourable properties for building local calibration models with new data.

5. Discussion

Upcoming satellite-borne missions aiming at forest AGB estimation require accurate calibration and validation plots across hectare scales to match their sensors' footprints. Laser scanning-based technologies offer the opportunity to assess forest AGB non-destructively and possibly with lower errors and biases than traditional inventory techniques. This study assessed strategies that make use of traditional, field-inventory based ASM, TLS and UAV-LS dense point clouds for individual tree AGB estimation.

5.1. Applying globally calibrated ASMs at local scales

Among the five implemented strategies, strategies Ia and Ib applied ASM that were calibrated on global, not site-specific data sets (Chave et al., 2014; Jucker et al., 2017; Forrester et al., 2017). These strategies have a relatively low demand in resources for the establishment of new local calibration and validation plots compared to strategies IIa/b/c, which involve local data collection and model development.

The errors at the individual tree level in terms of RMSE for strategy Ia found in this study were partly in line with published data, but also deviated strongly, depending on the site. When calculating an RMSE in linear space based on the data published by Chave et al. (2014), French Guinean and Australian trees achieve a RMSE of 0.48, 0.04 Mg, respectively, when using the ASM of Chave et al. (2014) (Eq. (3)). Strategy Ia at FG, RC and LF achieved errors of 0.60, 0.86, 0.42Mg, respectively (Fig. 11). Hence, the error for FG and RC was on the same

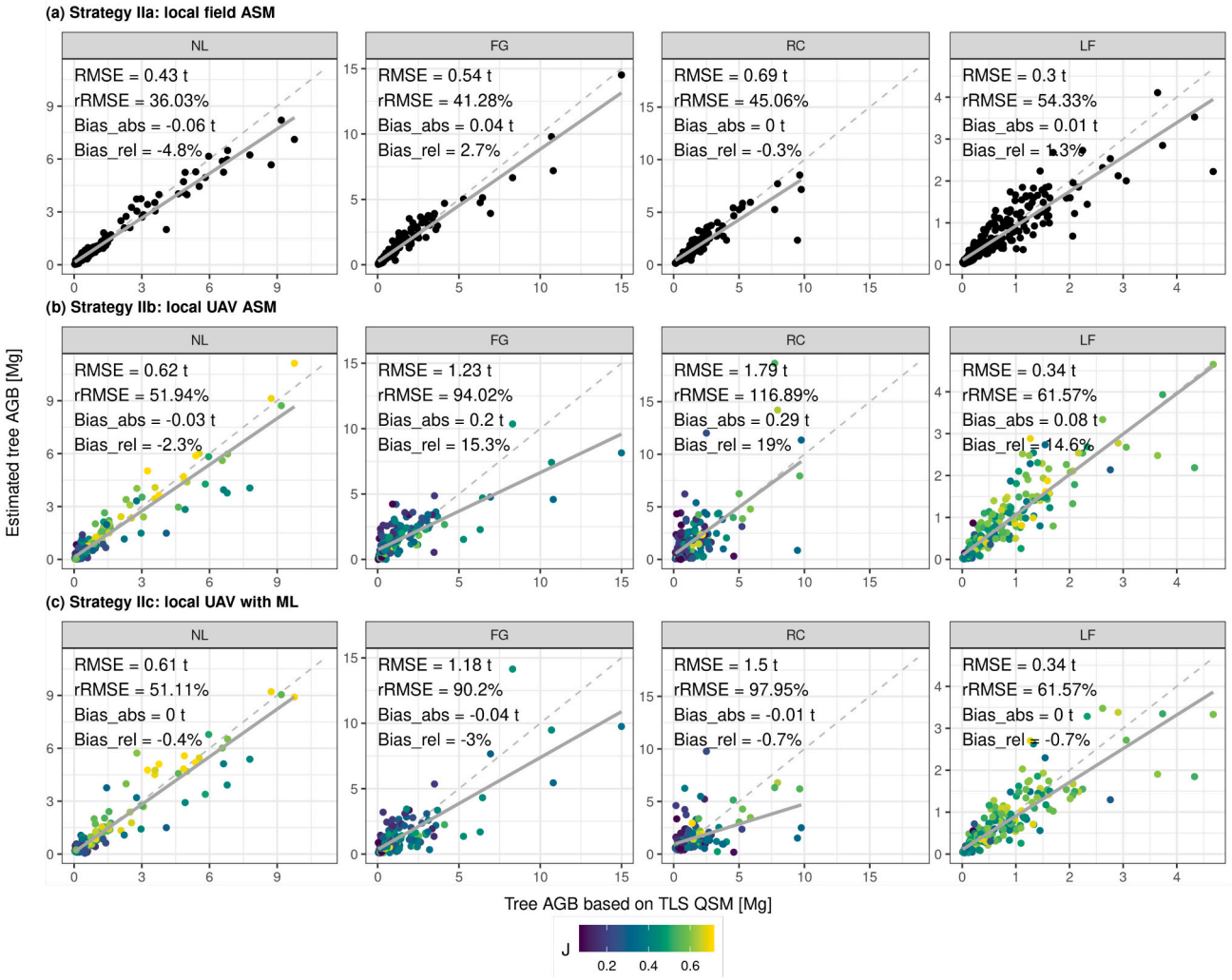

Fig. 12. Individual tree AGB estimation with modelling strategies based on combined TLS and UAV-LS data and local calibration. Points coloured according to their Jaccard index *J* of the UAV-LS tree with its respective TLS tree. All error metrics based on LOOCV. Grey dashed lines indicate 1:1 lines. Solid grey solid lines are linear trend models.

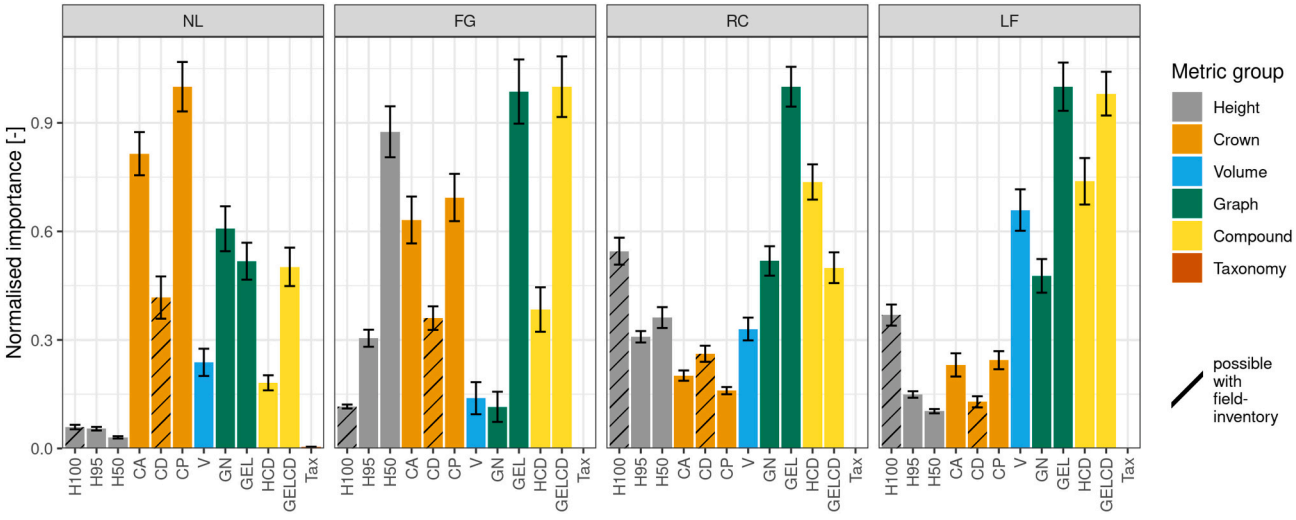

Fig. 13. Normalised random forest importance of individual UAV-LS tree metrics for strategy IIc across sites. Error bars represent standard deviation across the LOOCV models. Tax refers to taxonomic information (gymnosperm, angiosperm).

order of magnitude, but for LF was about ten times higher in this study than for the calibration data of Chave et al. (2014). On the other hand, strategy Ib, which implemented the global ASM developed by Jucker et al. (2017), achieved individual tree AGB RMSE of 1.29, 1.56, 1.26, 0.59 Mg for NL, FG, RC and LF, respectively, which were comparable to 1.70 Mg of Jucker et al. (2017).

However, the population bias for strategies Ia/b that ranged from −65.2-56.3% across sites might be more problematic, especially with the background of satellite calibration and validation in mind. Assuming that the used TLS estimates that were used for comparison here exhibit a bias of ±10% as judged by past studies (Section 1), the modelling strategies possibly induced a larger bias in the population estimates than the TLS estimation process. A problem here is that the TLS measured DBH and H100 exhibit different error distributions than their field-measured equivalents. Wang et al. (2019) highlighted the differences and possible biases between inventory and ALS measured individual tree heights, and concluded that ALS is more reliable in tall trees, while inventory measurements underestimate tall tree height. Coomes et al. (2017) found biases between inventory and ALS measured CA. This crossing of data modalities would make the application of field-calibrated ASM on LiDAR derived metrics problematic.

5.2. Calibration of traditional ASMs with TLS

Strategy IIa provided the overall lowest individual tree AGB RMSE for all sites except at LF. This underlines the potential of locally calibrated ASM. Additionally, it highlights the role of DBH as a powerful metric for individual tree AGB estimation (Chave et al., 2014; Forrester et al., 2017; Lau et al., 2019). Strategy IIb also included locally calibrated models, but implemented H100 and CD, which were not as well related to AGB (Fig. 10). Jucker et al. (2017) also found a smaller RMSE of 0.86 Mg for the Chave et al. (2014) pan-tropical ASM including DBH, when compared to their model with RMSE of 1.70 Mg based on H100 and CD.

Considering implementation opportunities, TLS has been discussed as a possible source for unbiased, non-destructive calibration data to supplement or even replace databases based on field measurements, especially with respect to large trees (Calders et al., 2015; Momo Takoudjou et al., 2018; Gonzalez de Tanago et al., 2018). Results of strategy IIa are supporting this argument. However, considering plot based estimations, i.e., aggregated estimates, the scaling primarily relying on DBH might invoke biases. A point that should also be taken into account for this strategy is cross-modal application of the calibrated ASM similar to strategies Ia/b: as strategy Ib was possibly experiencing biases due to application of a field measurement calibrated ASM on UAV-LS data, strategy IIa might result in biases during the application of the TLS calibrated ASM on field measurements. There are two possible countermeasures to overcome this problem: either, standardised, field-measured DBH and H100 that are collected alongside TLS acquisitions with standardised techniques and used for ASM calibration, or a generic correction factor is established based on the comparison of inventory and TLS metrics, and applied prior to calibration.

5.3. UAV-LS for tree-centric AGB estimation: point cloud segmentation

All five strategies implemented in this study were targeting a tree-centric AGB estimation, which means that AGB is estimated at the individual tree level before aggregation to plot scale. For plot scale analysis a full segmentation needs to be applied and the single trees' AGB summed up. In previous studies tree-centric approaches based on ALS achieved higher RMSE compared to area-based approaches (Ferraz et al., 2016; Coomes et al., 2017). The point cloud segmentation was identified as a bottleneck as either trees were wrongly segmented, or mostly in the case of understorey trees, omitted. Where these studies used point clouds with densities of 10.8 and 7.3 points/m^2 (Ferraz et al., 2016; Coomes et al., 2017), UAV-LS in this study could produce point clouds with ≥3700 points/m^2 (Table 1). Additionally, where Coomes et al. (2017) segmented the point clouds based on derived CHM, in this study a 3D graph-based segmentation algorithm exploiting the full point cloud was used (Raumonen et al., 2021). As a result understorey trees could be identified to a certain extent. However, their delineation was far from perfect as indicated by the comparison between manually checked trees (Section 4.1). Nonetheless, the combination of UAV-LS and 3D segmentation algorithms appears as a favourable pathway to realise tree-centric AGB estimation.

Concerning point cloud segmentation, it should be noted that the automatic UAV-LS segmentation was not analysed in full depth, i.e., spatially continuous comparison of the UAV-LS with a fully segmented TLS point cloud. This comparison would have produced on a tree by tree basis how many trees were not or wrongly detected. In fact, Martin-Ducup et al. (2021) identified the segmentation step as the weak link in automatic TLS based tree-centric volume estimation, which can also be expected for UAV-LS. The reason why the full accounting was not performed here is that a complete segmentation of the TLS point cloud with high quality is still extremely labour-intense. Even automatic approaches always require manual result control. For NL, FG and RC, this means several months more of human-hour input. However, such a full segmentation of the TLS data would enable the validation of plot based AGB, and full inter-comparison of area and tree-centric AGB modelling approaches, and should be tackled in future studies. Nonetheless, the accumulation of TLS trees to populations already showed very encouraging results that give a preview of full plot-scale results (Fig. 14). These results are interesting in particular because large trees were preferably sampled at FG and RC (Section 3.1), so that it can be expected that the bulk of plot AGB was contained in the tree TLS database.

5.4. UAV-LS for tree-centric AGB estimation: non-parametric modelling

Parametric approaches have been widely adopted as the preferred model framework for AGB estimation (Chave et al., 2014; Jucker et al., 2017; Coomes et al., 2017; Forrester et al., 2017). Due to their closed analytical form and few parameters, they deliver robust estimates already with few samples and are easy to understand in terms of effects of metrics on the estimate. However, recent works suggest that allometric relationships are not constant across tree size classes, in particular for DBH (Burt et al., 2020, 2021). This is especially a problem for the estimation of AGB in large trees, for which only few calibration samples exist due to the complexity of harvesting them in the field (Disney et al., 2018). As large trees play a major role in the forest AGB pool this ultimately leads to large biases at the plot scale, which is unacceptable for calibration purposes of satellite-based products.

In terms of modelling frameworks, Ploton et al. (2016) accounted for the size-variance with a nested model specifically accounting for crown biomass. Similarly, Zhou et al. (2021) developed a framework that dynamically adapts to varying relationship of stem AGB to total tree AGB across tree size classes. Another alternative to tackle the size-variance is to make use of a non-parametric estimation method as implemented in strategy IIc in this study. A particular advantage of non-parametric methods in this respect is their ability to be flexible to the metric-AGB response at different size classes. Instead of fitting a universal function across all sizes, non-parametric methods build on the provided calibration data to find the optimal relationships also as a function of the provided tree metrics. The fitting is supported by the provision of multiple tree metrics, which can be more or less useful at different size classes. The use of laser scanning technology like ALS or UAV-LS is crucial in this case as multiple metrics can be derived at once. Contrary, collecting multiple metrics during field inventories is making the process more complex and time-consuming.

Strategy IIc in this study implemented a non-parametric approach based on the RF model. Strategy IIc produced slightly lower individual tree AGB RMSE compared to the parametric strategy IIb and larger RMSE than the best strategy Ib. However, biases across sites could be

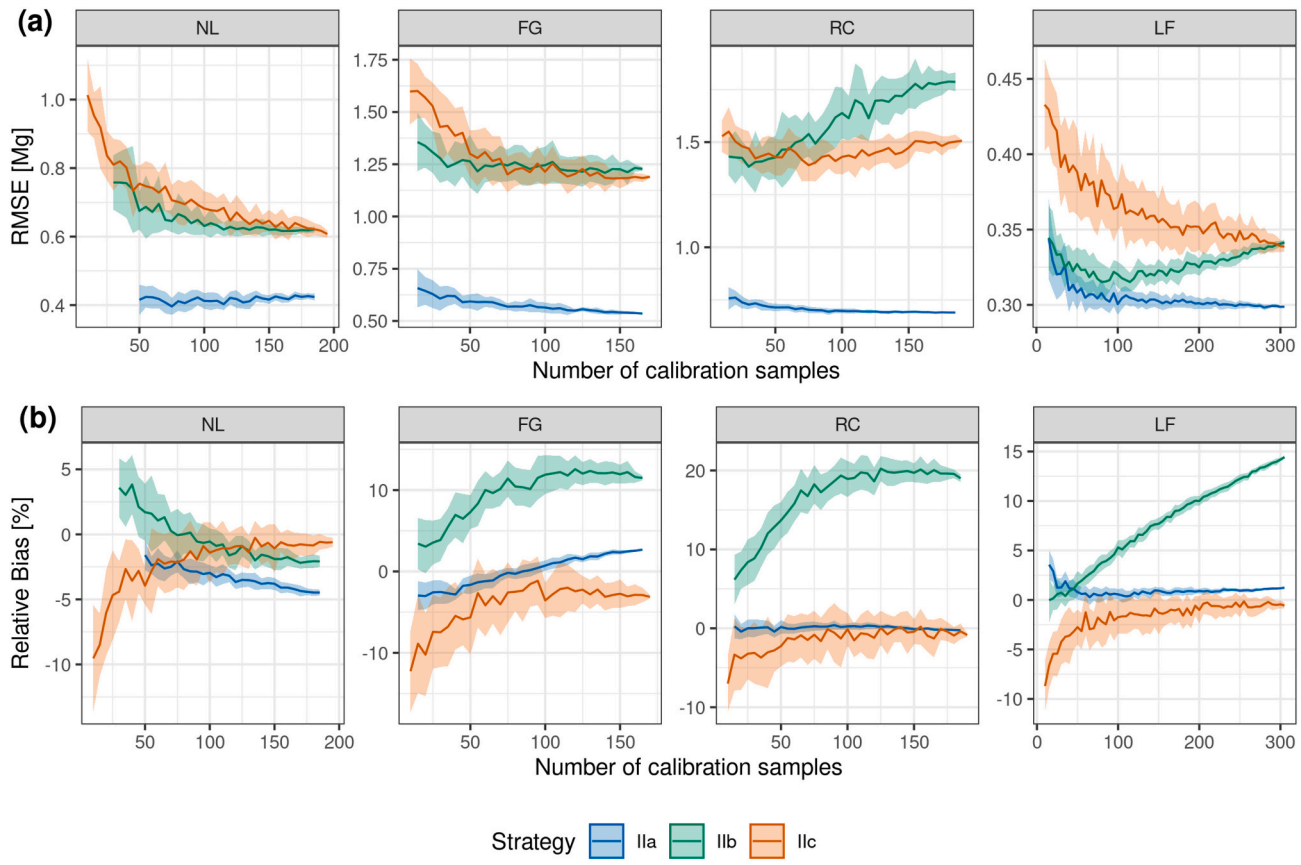

Fig. 14. Impact of calibration sample size on AGB prediction in terms of RMSE and relative bias for strategies IIa (local field ASM), IIb (local UAV ASM) and IIc (local UAV with machine learning).

reduced, which are relevant for satellite product calibration purposes. Similarly, Rudge et al. (2021) found that a non-parametric estimation method produced slightly larger RMSE but lower bias compared to a parametric approach when estimating DBH with UAV-LS CD and height. In this study, a minimum of 10–55 individual tree samples were necessary to calibrate the RF model to predict with bias of ≤5% (Fig. 14). Practically speaking, this number of trees is doable to scan with TLS within a two week campaign. Additional samples to check for possible over-fitting and independent cross-validation could be collected in similar time frames. Once sites are scanned with TLS UAV-LS, non-parametric learning approaches will be an attractive way to scale TLS to larger footprints, possibly to the extent of Committee on Earth Observation Satellites (CEOS) supersites (Chave et al., 2019; https://lpvs.gsfc.nasa.gov/LPV_Supersites/LPVsites.html). However, for site scale AGB estimation the influence of abiotic factors like water availability and soil properties should be taken into account for local model development (Ferry et al., 2010).

Additionally, ASM aim to be generic to a large geographic scale, e.g., species, landscape or biome scale. This is to make maximum use of the precious harvest samples and to be used in sites without harvest samples available. Non-parametric methods typically experience large uncertainties in parameter spaces that were not covered in the training data, i.e., extrapolation tasks. Nonetheless, in the context of calibration and validation, and proposed supersites (Chave et al., 2019) a local model with highest possible representativeness for the supersite and surroundings might be more valuable than a generic ASM. Here, the strength of non-parametric models lies in their high accuracy in local set ups, which is also discussed for other biophysical variable retrieval techniques such as leaf area index (LAI) and leaf chlorophyll content (Verrelst et al., 2015).

5.5. *UAV-LS for tree-centric AGB estimation: challenges and opportunities*

Among the modelling strategies applied in this study, strategies IIb/c make use of UAV-LS in combination with TLS data. The data acquisition with both sensor technologies has the highest requirements in terms of initial infrastructure investments, technology, logistics and legal requirements, primarily driven by the organisation of unoccupied aerial vehicleUAV flights. Flights might also not be possible at all forest sites particularly in dense canopies where the plots are far from take-off areas. This needs to be mitigated by targeting only suitable sites. As UAVs become more important in calibration and validation activities other than AGB (Brede et al., 2018; Origo et al., 2021; Niro et al., 2021), site maintainers will also have an interest in accommodating UAV flights by, for example, preparing take-off areas. Additionally, dense forests have higher requirements than sparse canopies on the UAV-LS scanner in terms of PRR, range and geo-location accuracy without the support of ground control targets. In particular, the effect of point cloud density on the estimation performance needs to be investigated in order to find a balance between number of flights and prediction performance for operational purposes.

However, once collected, dense UAV-LS point clouds can be used to estimate a range of individual tree metrics that are practically impossible to measure in field inventories (Section 3.3). Additionally, UAV-LS point clouds can potentially achieve a low absolute geo-location error of typically ≤1 m, when post-processing kinematic (PPK) methods are employed during the point cloud production (Brede et al., 2017; Almeida et al., 2019). This allows direct comparison with satellite products, which is typically a problem when using traditional field methods (Réjou-Méchain et al., 2019). Furthermore, once collected UAV-LS and TLS data can be re-analysed as new segmentation and

analysis procedures become available, also with respect to wood density estimation (Wilkes et al., 2021; Demol et al., 2021b; Åkerblom, Kaitaniemi, 2021).

One aspect that also needs further attention is the taxonomic classification of individual trees for the purpose of wood density determination. In this study, classification to the species and family level was possible at NL due to the spatially well separated stands, but only angiosperm and gymnosperm could be distinguished at other sites. High-resolution UAV based photography combined with deep learning (Schiefer et al., 2020), structural features (Terryn et al., 2020), and combined hyperspectral and structural features (Shi et al., 2018) derived from UAV acquired data alongside UAV-LS could contribute to usable methods for this challenge.

Finally, in order to draw conclusions on plot-based estimation capabilities of UAV-LS, a comprehensive analysis of UAV-LS segmentation performance needs to be conducted. This requires a full plot scale, quality controlled TLS individual tree segmentation and wood volume estimates. So far, TLS is the only means to adequately trace occupied canopy space back to individuals, thereby enabling to judge segmentation quality in 3D, but the process of TLS data preparation is very laborious and time-consuming.

6. Conclusions

Advances in terrestrial and UAV-based laser scanning provide the opportunity to produce fine detail point clouds of forests. New automatic point cloud segmentation routines enable to make use of these data for individual tree structure characterisation across hectares. This study made use of these data sources and routines to investigate different AGB modelling strategies that use either global or local calibration data, and parametric or non-parametric modelling approaches. Mixing data modalities by applying ASM calibrated with field inventory data resulted in biases especially for larger trees. The application of adjustment factors should be considered when translating between field-inventory and LiDAR metrics. Local calibration based on parametric modelling including DBH and tree height produced the lowest individual tree RMSE across sites, highlighting the power of direct trunk measurements for AGB estimation. This strategy could use TLS for calibration and field inventories for coverage of a supersite. On the other hand, local calibration based on UAV-LS derived metrics and non-parametric modelling resulted in relatively high individual tree AGB RMSE, but consistently low population bias within ±5%. A low bias is an important property when summing up individual tree AGB, as is necessary for satellite calibration and validation. This bias level was reached with 15–55 training samples, depending on site conditions, which can be relatively quickly collected with TLS. This approach can rapidly acquire hectare-scale data necessary for supersite characterisation. Compared to area-based ALS estimation approaches, the employed individual tree AGB modelling strategies have the advantage of being traceable to the individual tree and allow aggregation to arbitrary scales for flexible preparation of calibration and validation data for space-borne missions.

Data availability

UAV-LS and TLS data for the Speulderbos NL site are available at https://doi.org/10.4121/13061306.v1.

Declaration of Competing Interest

The authors declare that they have no known competing financial interests or personal relationships that could have appeared to influence the work reported in this paper.

Acknowledgements

This work was carried out as part of the IDEAS-QA4EO and Forest-Scan contracts funded by ESA-ESRIN. Fieldwork at the Speulderbos site was funded by the IDEAS+ contract funded by ESA-ESRIN. The Australian fieldwork was funded by BELSPO (Belgian Science Policy Office) in the frame of the STEREO III programme - project 3D-FOREST (SR/02/355).

Kim Calders was funded by the European Union's Horizon 2020 research and innovation programme under the Marie Sklodowska-Curie grant agreement No 835398. Sruthi M. Krishna Moorthy was funded by BELSPO (Belgian Science Policy Office) in the frame of the STEREO III programme – project 3D-FOREST (SR/02/355). Di Wang was supported by the National Key R&D Program of China (2021YFF0704600) and the National Natural Science Foundation of China under Grant No. 42101330.

The authors want to thank Diego Marcos Gonzalez for helpful discussions on modelling paradigms. The access to the RiCOPTER was made possible by Shared Research Facilities of Wageningen University Research. The authors thank the Dutch Forestry Service (Staatsbosbeheer) for granting access to the Speulderbos site. This work was supported by the use of Terrestrial Ecosystem Research Network (TERN) infrastructure, which is enabled by the Australian Government's National Collaborative Research Infrastructure Strategy (NCRIS).

The authors thank three anonymous reviewers for critical and constructive remarks that helped to improve the quality of the manuscript.

Appendix A. UAV-LS segmentation parameters

Table A.7
Parameter values used for the automatic segmentation routine for the UAV-LS point cloud (Raumonen et al., 2021).

	NL	FG	RC	LF
Patch diameter [m]	0.2	0.2	0.2	0.2
Initial gap size [m]	0.1	0.1	0.2	0.2
Base layer height [m]	2.5	2.5	2.5	2.5
Length/Height ratio [–]	1.3	1.3	1.3	1.3

References

Åkerblom, M., Kaitaniemi, P., 2021. Terrestrial laser scanning: a new standard of forest measuring and modelling? Annal. Bot. 128 (6), 1–9.

Almeida, D., Broadbent, E., Zambrano, A., Wilkinson, B., Ferreira, M., Chazdon, R., Meli, P., Gorgens, E., Silva, C., Stark, S., Valbuena, R., Papa, D., Brancalion, P., 2018. Monitoring the structure of forest restoration plantations with a drone-LiDAR system. Int. J. Appl. Earth Observ. Geoinf. 79, 192–198. https://doi.org/10.1016/j.jag.2019.03.014.

Asner, G.P., Mascaro, J., 2014. Mapping tropical forest carbon: calibrating plot estimates to a simple LiDAR metric. Remote Sens. Environ. 140, 614–624. https://linkinghub.elsevier.com/retrieve/pii/S003442571300360X.
Baskerville, G.L., 1972. Use of logarithmic regression in the estimation of plant biomass. Can. J. Forest Res. 2 (1), 49–53.
Belgiu, M., Drăgu, L., 2016. Random forest in remote sensing: a review of applications and future directions. ISPRS J. Photogram. Rem. Sens. 114, 24–31.
Bradford, M., Murphy, H.T., 2019. The importance of large-diameter trees in the wet tropical rainforests of Australia. Plos One 14 (5), e0208377. https://doi.org/10.1371/journal.pone.0208377.
Bradford, M.G., Metcalfe, D.J., Ford, A., Liddell, M.J., McKeown, A., 2014. Floristics, stand structure and aboveground biomass of a 25-ha rainforest plot in the wet tropics of Australia. J. Trop. Forest Sci. 26, 543–553.
Brede, B., Bartholomeus, H., Suomalainen, J., Clevers, J., Verbesselt, J., Herold, M., Culvenor, D., Gascon, F., 2016. The speulderbos fiducial reference site for continuous monitoring of forest biophysical variables. In: Living Planet Symposium. Prague, Czech Republic, 9–13 May 2016. Prague, p. 5.
Brede, B., Calders, K., Lau, A., Raumonen, P., Bartholomeus, H.M., Herold, M., Kooistra, L., 2019. Non-destructive tree volume estimation through quantitative structure modelling: comparing UAV laser scanning with terrestrial LiDAR. Remote Sens. Environ. 233, 111355. https://doi.org/10.1016/j.rse.2019.111355.
Brede, B., Lau, A., Bartholomeus, H.M., Kooistra, L., 2017. Comparing riegl RiCOPTER UAV LiDAR derived canopy height and DBH with terrestrial LiDAR. Sensors 17 (10), 2371. http://www.mdpi.com/1424-8220/17/10/2371.
Brede, B., Lau Sarmiento, A.A., Raumonen, P., Bartholomeus, H., Herold, M., Kooistra, L., 2020. Speulderbos terrestrial TLS and unmanned aerial vehicle laser scanning UAV-LS 2017. https://data.4tu.nl/articles/dataset/Speulderbos_Terrestrial_TLS_and_Unmanned_Aerial_Vehicle_Laser_Scanning_UAV-LS_2017/13061306/1.
Brede, B., Suomalainen, J., Roosjen, P.P., Aasen, H., Kooistra, L., Bartholomeus, H.M., Clevers, J.G., Herold, M., 2018. Opportunities of UAV based sensing for vegetation land product validation. In: Land Product Validation and Evolution. Frascati, Italy.
Breiman, L., 2001. Random forests. Mach. Learn. 45 (1), 5–32.
Burt, A., Boni Vicari, M., da Costa, A.C.L., Coughlin, I., Meir, P., Rowland, L., Disney, M., 2021. New insights into large tropical tree mass and structure from direct harvest and terrestrial LiDAR. Royal Soc. Open Sci. 8 (2) https://doi.org/10.1098/rsos.201458 rsos.201458.
Burt, A., Calders, K., Cuni-Sanchez, A., Gómez-Dans, J., Lewis, P., Lewis, S.L., Malhi, Y., Phillips, O.L., Disney, M., 2020. Assessment of bias in pan-tropical biomass predictions. Front. Forests Global Change 3.
Calders, K., Disney, M.I., Armston, J., Burt, A., Brede, B., Origo, N., Muir, J., Nightingale, J., 2017. Evaluation of the range accuracy and the radiometric calibration of multiple terrestrial laser SCANNING instruments for data interoperability. IEEE Trans. Geosci. Remote Sensing 55 (5), 2716–2724. http://ieeexplore.ieee.org/document/7858757/.
Calders, K., Newnham, G., Burt, A., Murphy, S., Raumonen, P., Herold, M., Culvenor, D., Avitabile, V., Disney, M., Armston, J., Kaasalainen, M., 2015. Nondestructive estimates of above-ground biomass using terrestrial laser scanning. Methods Ecol. Evol. 6 (2), 198–208. https://doi.org/10.1111/2041-210X.12301.
Chave, J., Andalo, C., Brown, S., Cairns, M.A., Chambers, J.Q., Eamus, D., Fölster, H., Fromard, F., Higuchi, N., Kira, T., Lescure, J.-P., Nelson, B.W., Ogawa, H., Puig, H., Riéra, B., Yamakura, T., 2005. Tree allometry and improved estimation of carbon stocks and balance in tropical forests. Oecologia 145 (1), 87–99. https://doi.org/10.1007/s00442-005-0100-x.
Chave, J., Condit, R., Aguilar, S., Hernandez, A., Lao, S., Perez, R., 2004. Error propagation and scaling for tropical forest biomass estimates. Philosph. Trans. Royal Soc. B: Biol. Sci. 359 (1443), 409–420.
Chave, J., Coomes, D., Jansen, S., Lewis, S.L., Swenson, N.G., Zanne, A.E., 2009. Towards a worldwide wood economics spectrum. Ecol. Lett. 12 (4), 351–366. https://doi.org/10.1111/j.1461-0248.2009.01285.x.
Chave, J., Davies, S.J., Phillips, O.L., Lewis, S.L., Sist, P., Schepaschenko, D., Armston, J., Baker, T.R., Coomes, D., Disney, M., Duncanson, L., Hérault, B., Labrière, N., Meyer, V., Réjou-Méchain, M., Scipal, K., Saatchi, S., 2019. Ground data are essential for biomass remote sensing missions. Surveys Geophys. 40 (4), 863–880. https://doi.org/10.1007/s10712-019-09528-w.
Chave, J., Réjou-Méchain, M., Búrquez, A., Chidumayo, E., Colgan, M.S., Delitti, W.B., Duque, A., Eid, T., Fearnside, P.M., Goodman, R.C., Henry, M., Martínez-Yrízar, A., Mugasha, W.A., Muller-Landau, H.C., Mencuccini, M., Nelson, B.W., Ngomanda, A., Nogueira, E.M., Ortiz-Malavassi, E., Pélissier, R., Ploton, P., Ryan, C.M., Saldarriaga, J.G., Vieilledent, G., 2014. Improved allometric models to estimate the aboveground biomass of tropical trees. Global Change Biol. 20 (10), 3177–3190.
Coomes, D.A., Dalponte, M., Jucker, T., Asner, G.P., Banin, L.F., Burslem, D.F., Lewis, S. L., Nilus, R., Phillips, O.L., Phua, M.H., Qie, L., 2017. Area-based vs tree-centric approaches to mapping forest carbon in Southeast Asian forests from airborne laser scanning data. Remote Sens. Environ. 194, 77–88. https://doi.org/10.1016/j.rse.2017.03.017.
Dalponte, M., Coomes, D.A., 2016. Tree-centric mapping of forest carbon density from airborne laser scanning and hyperspectral data. Methods Ecol. Evol. 7 (10), 1236–1245.
de Oliveira, L.F.R., Lassiter, H.A., Wilkinson, B., Whitley, T., Ifju, P., Logan, S.R., Peter, G.F., Vogel, J.G., Martin, T.A., 2021. Moving to automated tree inventory: comparison of UAS-derived LiDAR and photogrammetric data with manual ground estimates. Remote Sens. 13 (1), 1–16.
Demol, M., Calders, K., Krishna Moorthy, S.M., Van den Bulcke, J., Verbeeck, H., Gielen, B., 2021a. Consequences of vertical basic wood density variation on the estimation of aboveground biomass with terrestrial laser scanning. Trees 35 (2), 671–684. https://doi.org/10.1007/s00468-020-02067-7, 0123456789.
Demol, M., Calders, K., Verbeeck, H., Gielen, B., 2021b. Forest above-ground volume assessments with terrestrial laser scanning: a ground-truth validation experiment in temperate, managed forests. Annal. Bot. 128 (6), 805–819.
Demol, M., Wilkes, P., Raumonen, P., Krishna Moorthy, S., Calders, K., Gielen, B., Verbeeck, H., 2022. Volumetric overestimation of small branches in 3D reconstructions of Fraxinus excelsior. Silva Fennica 56 (1). https://www.silvafennica.fi/article/10550.
Disney, M.I., Boni Vicari, M., Burt, A., Calders, K., Lewis, S.L., Raumonen, P., Wilkes, P., 2018. Weighing trees with lasers: advances, challenges and opportunities. Inter. Focus 8 (2). https://doi.org/10.1098/rsfs.2017.0048, 20170048.
Drake, J.B., Dubayah, R.O., Clark, D.B., Knox, R.G., Blair, J., Hofton, M.A., Chazdon, R. L., Weishampel, J.F., Prince, S., 2002. Estimation of tropical forest structural characteristics using large-footprint LiDAR. Remote Sens. Environ. 79 (2–3), 305–319. http://linkinghub.elsevier.com/retrieve/pii/S0034425701002814.
Duncanson, L., Armston, J., Disney, M., Avitabile, V., Barbier, N., Calders, K., Carter, S., Chave, J., Herold, M., Crowther, T.W., Falkowski, M., Kellner, J.R., Labrière, N., Lucas, R., MacBean, N., McRoberts, R.E., Meyer, V., Næ, E., Nickeson, J.E., Paul, K.I., Phillips, O.L., Réjou-Méchain, M., Román, M., Roxburgh, S., Saatchi, S., Schepaschenko, D., Scipal, K., Siqueira, P.R., Whitehurst, A., Williams, M., 2019. The importance of consistent global forest aboveground biomass product validation. Surveys Geophys. 40 (4), 979–999. https://doi.org/10.1007/s10712-019-09538-8, 0123456789.
Duncanson, L., Kellner, J.R., Armston, J., Dubayah, R., Minor, D.M., Hancock, S., Healey, S.P., Patterson, P.L., Saarela, S., Marselis, S., Silva, C.E., Bruening, J., Goetz, S.J., Tang, H., Hofton, M., Blair, B., Luthcke, S., Fatoyinbo, L., Abernethy, K., Alonso, A., Andersen, H.E., Aplin, P., Baker, T.R., Barbier, N., Bastin, J.F., Biber, P., Boeckx, P., Bogaert, J., Boschetti, L., Boucher, P.B., Boyd, D.S., Burslem, D.F., Calvo-Rodriguez, S., Chave, J., Chazdon, R.L., Clark, D.B., Clark, D.A., Cohen, W.B., Coomes, D.A., Corona, P., Cushman, K.C., Cutler, M.E., Dalling, J.W., Dalponte, M., Dash, J., de Miguel, S., Deng, S., Ellis, P.W., Erasmus, B., Fekety, P.A., Fernandez-Landa, A., Ferraz, A., Fischer, R., Fisher, A.G., García-Abril, A., Gobakken, T., Hacker, J.M., Heurich, M., Hill, R.A., Hopkinson, C., Huang, H., Hubbell, S.P., Hudak, A.T., Huth, A., Imbach, B., Jeffery, K.J., Katoh, M., Kearsley, E., Kenfack, D., Kljun, N., Knapp, N., Král, K., Kruček, M., Labrière, N., Lewis, S.L., Longo, M., Lucas, R.M., Main, R., Manzanera, J.A., Martínez, R.V., Mathieu, R., Memiaghe, H., Meyer, V., Mendoza, A.M., Monerris, A., Montesano, P., Morsdorf, F., Næ, E., Naidoo, L., Nilus, R., O'Brien, M., Orwig, D.A., Papathanassiou, K., Parker, G., Philipson, C., Phillips, O.L., Pisek, J., Poulsen, J.R., Pretzsch, H., Rüdiger, C., Saatchi, S., Sanchez-Azofeifa, A., Sanchez-Lopez, N., Scholes, R., Silva, C.A., Simard, M., Skidmore, A., Stereńczak, K., Tanase, M., Torresan, C., Valbuena, R., Verbeeck, H., Vrska, T., Wessels, K., White, J.C., White, L.J., Zahabu, E., Zgraggen, C., 2022. Aboveground biomass density models for NASA's global ecosystem dynamics investigation (GEDI) LiDAR mission. Remote Sens. Environ. 270.
Duncanson, L., Rourke, O., Dubayah, R., 2015. Small sample sizes yield biased allometric equations in temperate forests. Sci. Rep. 5, 1–13.
Ferraz, A., Saatchi, S., Mallet, C., Meyer, V., 2016. LiDAR detection of individual tree size in tropical forests. Remote Sens. Environ. 183, 318–333. https://doi.org/10.1016/j.rse.2016.05.028.
Ferry, B., Morneau, F., Bontemps, J.D., Blanc, L., Freycon, V., 2010. Higher treefall rates on slopes and waterlogged soils result in lower stand biomass and productivity in a tropical rain forest. J. Ecol. 98 (1), 106–116.
Forrester, D.I., Tachauer, I.H., Annighoefer, P., Barbeito, I., Pretzsch, H., Ruiz-Peinado, R., Stark, H., Vacchiano, G., Zlatanov, T., Chakraborty, T., Saha, S., Sileshi, G.W., 2017. Generalized biomass and leaf area allometric equations for European tree species incorporating stand structure, tree age and climate. Forest Ecol. Manag. 396, 160–175. https://doi.org/10.1016/j.foreco.2017.04.011.
Gonzalez de Tanago, J., Lau, A., Bartholomeus, H., Herold, M., Avitabile, V., Raumonen, P., Martius, C., Goodman, R.C., Disney, M., Manuri, S., Burt, A., Calders, K., 2018. Estimation of above-ground biomass of large tropical trees with terrestrial LiDAR. Methods Ecol. Evol. 9 (2), 223–234. https://doi.org/10.1111/2041-210X.12904.
Guo, Q., Su, Y., Hu, T., Zhao, X., Wu, F., Li, Y., Liu, J., Chen, L., Xu, G., Lin, G., Zheng, Y., Lin, Y., Mi, X., Fei, L., Wang, X., 2017. An integrated UAV-borne LiDAR system for 3D habitat mapping in three forest ecosystems across China. Int. J. Remote Sens. 38 (8–10), 1–19. https://doi.org/10.1080/01431161.2017.1285083.
Hackenberg, J., Wassenberg, M., Spiecker, H., Sun, D., 2015. Non destructive method for biomass prediction combining TLS derived tree volume and wood density. Forests 6 (4), 1274–1300.
Hilker, T., van Leeuwen, M., Coops, N.C., Wulder, M.A., Newnham, G.J., Jupp, D.L.B., Culvenor, D.S., 2010. Comparing canopy metrics derived from terrestrial and airborne laser scanning in a douglas-fir dominated forest stand. Trees 24 (5), 819–832. https://doi.org/10.1007/s00468-010-0452-7.
Jaakkola, A., Hyyppä, J., Kukko, A., Yu, X., Kaartinen, H., Lehtomäki, M., Lin, Y., 2010. A low-cost multi-sensoral mobile mapping system and its feasibility for tree measurements. ISPRS J. Photogram. Rem. Sens. 65 (6), 514–522. https://doi.org/10.1016/j.isprsjprs.2010.08.002.
Jaccard, P., 1912. The distribution of the flora in the alpine zone. New Phytologist 11 (2), 37–50.
Joyce, K.E., Anderson, K., Bartolo, R.E., 2021. Of Course we fly unmanned-we're women! Drones 5 (1), 21.
Jucker, T., Caspersen, J., Chave, J., Antin, C., Barbier, N., Bongers, F., Dalponte, M., van Ewijk, K.Y., Forrester, D.I., Haeni, M., Higgins, S.I., Holdaway, R.J., Iida, Y., Lorimer, C., Marshall, P.L., Momo, S., Moncrieff, G.R., Ploton, P., Poorter, L., Rahman, K.A., Schlund, M., Sonké, B., Sterck, F.J., Trugman, A.T., Usoltsev, V.A., Vanderwel, M.C., Waldner, P., Wedeux, B.M., Wirth, C., Wöll, H., Woods, M.,

Xiang, W., Zimmermann, N.E., Coomes, D.A., 2017. Allometric equations for integrating remote sensing imagery into forest monitoring programmes. Global Change Biol. 23 (1), 177–190.
Knapp, N., Huth, A., Fischer, R., 2021. Tree crowns cause border effects in area-based biomass estimations from remote sensing. Remote Sens. 13 (8), 1592.
Kuželka, K., Slavík, M., Surový, P., 2020. Very high density point clouds from UAV laser scanning for automatic tree stem detection and direct diameter measurement. Remote Sens. 12 (8), 1236. https://www.mdpi.com/2072-4292/12/8/1236.
Lau, A., Calders, K., Bartholomeus, H., Martius, C., Raumonen, P., Herold, M., Vicari, M., Sukhdeo, H., Singh, J., Goodman, R.C., 2019. Tree biomass equations from terrestrial LiDAR: a case study in Guyana. Forests 10 (6), 1–18.
Levick, S.R., Whiteside, T., Loewensteiner, D.A., Rudge, M., Bartolo, R., 2021. Leveraging TLS as a calibration and validation tool for MLS and ULS mapping of savanna structure and biomass at landscape-scales. Remote Sens. 13 (2), 257. https://www.mdpi.com/2072-4292/13/2/257.
Liu, K., Shen, X., Cao, L., Wang, G., Cao, F., 2018. Estimating forest structural attributes using UAV-LiDAR data in Ginkgo plantations. ISPRS J. Photogram. Rem. Sens. 146, 465–482. https://doi.org/10.1016/j.isprsjprs.2018.11.001.
Luck, L., Hutley, L.B., Calders, K., Levick, S.R., 2020. Exploring the variability of tropical savanna tree structural allometry with terrestrial laser scanning. Remote Sens. 12 (23), 1–16.
Mandlburger, G., Hollaus, M., Glira, P., Wieser, M., Riegl, U., Pfennigbauer, M., 2015. First examples from the RIEGL VUX-SYS for forestry applications.. In: Proceedings of Silvilaser. La Grande Motte, France, pp. 105–107.
Martin-Ducup, O., Mofack, G., Wang, D., Raumonen, P., Ploton, P., Sonké, B., Barbier, N., Couteron, P., Pélissier, R., 2021. Evaluation of automated pipelines for tree and plot metric estimation from TLS data in tropical forest areas. Annal. Bot. 128 (6), 753–766. https://doi.org/10.1080/07853890.2020.1840620.
Mascaro, J., Detto, M., Asner, G.P., Muller-Landau, H.C., 2011. Evaluating uncertainty in mapping forest carbon with airborne LiDAR. Remote Sens. Environ. 115 (12), 3770–3774. https://doi.org/10.1016/j.rse.2011.07.019.
Meyer, V., Saatchi, S., Clark, D.B., Keller, M., Vincent, G., Ferraz, A., Espírito-Santo, F., D'Oliveira, M.V., Kaki, D., Chave, J., 2018. Canopy area of large trees explains aboveground biomass variations across neotropical forest landscapes. Biogeosciences 15 (11), 3377–3390.
Momo, S.T., Ploton, P., Martin-Ducup, O., Lehnebach, R., Fortunel, C., Sagang, L.B.T., Boyemba, F., Couteron, P., Fayolle, A., Libalah, M., Loumeto, J., Medjibe, V., Ngomanda, A., Obiang, D., Pélissier, R., Rossi, V., Yongo, O., Sonké, B., Barbier, N., 2020. Leveraging signatures of plant functional strategies in wood density profiles of African trees to correct mass estimations from terrestrial laser data. Sci. Rep. 10 (1), 2001. http://www.nature.com/articles/s41598-020-58733-w.
Momo Takoudjou, S., Ploton, P., Sonké, B., Hackenberg, J., Griffon, S., de Coligny, F., Kamdem, N.G., Libalah, M., Mofack, G.I., Le Moguédec, G., Pélissier, R., Barbier, N., 2018. Using terrestrial laser scanning data to estimate large tropical trees biomass and calibrate allometric models: a comparison with traditional destructive approach. Methods Ecol. Evol. 9 (4), 905–916. https://doi.org/10.1111/2041-210X.12933.
Niro, F., Goryl, P., Dransfeld, S., Boccia, V., Gascon, F., Adams, J., Themann, B., Scifoni, S., Doxani, G., 2021. European space agency (ESA) calibration/validation strategy for optical land-imaging satellites and pathway towards interoperability. Remote Sens. 13 (15), 3003. https://www.mdpi.com/2072-4292/13/15/3003.
Origo, N., Morrone, R., Sinclair, M., Maclellan, C., Nightingale, J., Gorro no, J., Honkavaara, E., Hakala, T., Nevalainen, O., 2021. UAV-Based hyperspectral data for surface reflectance fiducialreference measurements (FRM). In: IGARSS 2021 International Geoscience and Remote Sensing Symposium, July 12-16, Brussels. Brussels.
Phillips, O.L., Sullivan, M.J.P., Baker, T.R., Monteagudo Mendoza, A., Vargas, P.N., Vásquez, R., 2019. Species matter: wood density influences tropical forest biomass at multiple scales. Surveys Geophys. 40 (4), 913–935. https://doi.org/10.1007/s10712-019-09540-0.
Picard, N., Saint-André, L., Henry, M., 2012. Manual for building tree volume and biomass allometric equations: from field measurement to prediction. Food and Agriculture rganization of the United Nations, Rome, and Centre de Coopération Internationale en Recherche Agronomique pour le Développement, Montpellier, Rome, Montpellier.
Ploton, P., Barbier, N., Takoudjou Momo, S., Réjou-Méchain, M., Boyemba Bosela, F., Chuyong, G., Dauby, G., Droissart, V., Fayolle, A., Goodman, R.C., Henry, M., Kamdem, N.G., Mukirania, J.K., Kenfack, D., Libalah, M., Ngomanda, A., Rossi, V., Sonké, B., Texier, N., Thomas, D., Zebaze, D., Couteron, P., Berger, U., Pélissier, R., 2016. Closing a gap in tropical forest biomass estimation: taking crown mass variation into account in pantropical allometries. Biogeosciences 13 (5), 1571–1585. https://www.biogeosciences.net/13/1571/2016/.
Puliti, S., Breidenbach, J., Astrup, R., 2020. Estimation of forest growing stock volume with uav laser scanning data: can it be done without field data? Remote Sens. 12 (8), 1245. https://www.mdpi.com/2072-4292/12/8/1245.
Raumonen, P., Brede, B., Lau, A., Bartholomeus, H., 2021. A shortest path based tree isolation method for UAV LiDAR data. In: IGARSS 2021 International Geoscience and Remote Sensing Symposium, July 12-16, Brussels. Brussels.
Raumonen, P., Casella, E., Calders, K., Murphy, S., Åkerbloma, M., Kaasalainen, M., 2015. Massive-scale tree modelling from TLS data. ISPRS annals of photogrammetry. Remote Sens. Spatial Inf. Sci. II-3/W4 189–196. http://www.isprs-ann-photogramm-remote-sens-spatial-inf-sci.net/II-3-W4/189/2015/.
Raumonen, P., Kaasalainen, M., Åkerblom, M., Kaasalainen, S., Kaartinen, H., Vastaranta, M., Holopainen, M., Disney, M., Lewis, P., 2013. Fast automatic precision tree models from terrestrial laser scanner data. Remote Sens. 5, 491–520. http://www.mdpi.com/2072-4292/5/2/491/.
Réjou-Méchain, M., Barbier, N., Couteron, P., Ploton, P., Vincent, G., Herold, M., Mermoz, S., Saatchi, S., Chave, J., de Boissieu, F., Féret, J.B., Takoudjou, S.M., Pélissier, R., 2019. Upscaling Forest Biomass from Field to Satellite Measurements: Sources of Errors and Ways to Reduce Them. Vol. 40. Springer, Netherlands. https://doi.org/10.1007/s10712-019-09532-0.
Réjou-Méchain, M., Tanguy, A., Piponiot, C., Chave, J., Hérault, B., 2017. BIOMASS: an R package for estimating above-ground biomass and its uncertainty in tropical forests. Methods Ecol. Evol. 8 (9), 1163–1167. https://onlinelibrary.wiley.com/doi/abs/10.1111/2041-210X.12753.
Rudge, M.L., Levick, S.R., Bartolo, R.E., Erskine, P.D., 2021. Modelling the diameter distribution of savanna trees with drone-based LiDAR. Remote Sens. 13 (7), 1–18.
Schiefer, F., Kattenborn, T., Frick, A., Frey, J., Schall, P., Koch, B., Schmidtlein, S., 2020. Mapping forest tree species in high resolution UAV-based RGB-imagery by means of convolutional neural networks. ISPRS J. Photogram. Rem. Sens. 170, 205–215. https://doi.org/10.1016/j.isprsjprs.2020.10.015.
Shi, Y., Skidmore, A.K., Wang, T., Holzwarth, S., Heiden, U., Pinnel, N., Zhu, X., Heurich, M., 2018. Tree species classification using plant functional traits from LiDAR and hyperspectral data. Int. J. Appl. Earth Observ. Geoinf. 73, 207–219. https://doi.org/10.1016/j.jag.2018.06.018.
Stovall, A.E.L., Vorster, A.G., Anderson, R.S., Evangelista, P.H., Shugart, H.H., 2017. Non-destructive aboveground biomass estimation of coniferous trees using terrestrial LiDAR. Remote Sens. Environ. 200, 31–42. https://doi.org/10.1016/j.rse.2017.08.013.
Terryn, L., Calders, K., Bartholomeus, H., Bartolo, R.E., Brede, B., D'hont, B., Disney, M., Herold, M., Lau, A., Shenkin, A., Whiteside, T.G., Wilkes, P., Verbeeck, H., 2022. Quantifying tropical forest structure through terrestrial and UAV laser scanning fusion in Australian rainforests. Remote Sens. Environ. 271, 112912. https://linkinghub.elsevier.com/retrieve/pii/S0034425722000268.
Terryn, L., Calders, K., Disney, M., Origo, N., Malhi, Y., Newnham, G., Raumonen, P., Åkerblom, M., Verbeeck, H., 2020. Tree species classification using structural features derived from terrestrial laser scanning. ISPRS J. Photogram. Rem. Sens. 168, 170–181.
van der Zee, J., Lau, A., Shenkin, A., 2021. Understanding crown shyness from a 3-D perspective. Annal. Bot. 128 (6), 1–38. https://doi.org/10.1093/aob/mcab035/6170584.
Vandendaele, B., Fournier, R.A., Vepakomma, U., Pelletier, G., Lejeune, P., Martin-Ducup, O., 2021. Estimation of northern hardwood forest inventory attributes using UAV laser scanning (ULS): transferability of laser scanning methods and comparison of automated approaches at the tree- and stand-level. Remote Sens. 13 (14), 2796.
Verrelst, J., Camps-Valls, G., Mu noz-Marí, J., Rivera, J.P., Veroustraete, F., Clevers, J.G., Moreno, J., 2015. Optical remote sensing and the retrieval of terrestrial vegetation bio-geophysical properties - A review. ISPRS J. Photogram. Rem. Sens. 108, 273–290. http://linkinghub.elsevier.com/retrieve/pii/S0924271615001422.
Wallace, L., Lucieer, A., Watson, C., Turner, D., 2012. Development of a UAV-LiDAR system with application to forest inventory. Remote Sens. 4 (6), 1519–1543.
Wallace, L., Lucieer, A., Watson, C.S., 2014. Evaluating tree detection and segmentation routines on very high resolution UAV LiDAR data. IEEE Trans. Geosci. Remote Sensing 52 (12), 7619–7628.
Wang, D., 2020. Unsupervised semantic and instance segmentation of forest point clouds. ISPRS J. Photogram. Rem. Sens. 165, 86–97. https://linkinghub.elsevier.com/retrieve/pii/S0924271620301180.
Wang, Y., Lehtomäki, M., Liang, X., Pyörälä, J., Kukko, A., Jaakkola, A., Liu, J., Feng, Z., Chen, R., Hyyppä, J., 2019. Is field-measured tree height as reliable as believed - a comparison study of tree height estimates from field measurement, airborne laser scanning and terrestrial laser scanning in a boreal forest. ISPRS J. Photogram. Rem. Sens. 147, 132–145. https://linkinghub.elsevier.com/retrieve/pii/S0924271618303046.
Wieser, M., Mandlburger, G., Hollaus, M., Otepka, J., Glira, P., Id, N.P., 2017. A case study of uas borne laser scanning for measurement of tree stem diameter. Remote Sens. 9 (11), 1–11.
Wilkes, P., Lau, A., Disney, M.I., Calders, K., Burt, A., Gonzalez de Tanago, J., Bartholomeus, H., Brede, B., Herold, M., 2017. Data acquisition considerations for terrestrial laser scanning of forest plots. Remote Sens. Environ. 196, 140–153. https://doi.org/10.1016/j.rse.2017.04.030.
Wilkes, P., Shenkin, A., Disney, M., Malhi, Y., Bentley, L.P., Vicari, M.B., 2021. Terrestrial laser scanning to reconstruct branch architecture from harvested branches. Methods Ecol. Evolu. 2021 12 (12), 1–14.
Wright, M.N., Ziegler, A., 2017. ranger: a fast implementation of random forests for high dimensional data in C++ and R. J. Stat. Software 77 (1). http://www.jstatsoft.org/v77/i01/.
Zanne, A.E., Lopez-Gonzalez, G., Coomes, D.A., Ilic, J., Jansen, S., Lewis, S.L., Miller, R. B., Swenson, N.G., Wiemann, M.C., Chave, J., 2009. Data from: towards a worldwide wood economics spectrum, Dryad. Dataset. https://doi.org/10.5061/dryad.234.
Zhou, X., Yang, M., Liu, Z., Li, P., Xie, B., Peng, C., 2021. Dynamic allometric scaling of tree biomass and size. Nature Plants 7 (1), 42–49. https://doi.org/10.1038/s41477-020-00815-8.